UNIVERSITÀ DEGLI STUDI DI NAPOLI

FEDERICO II

Dipartimento di Farmacia

CORSO DI LAUREA MAGISTRALE IN

BIOTECNOLOGIE DEL FARMACO

TESI DI LAUREA SPERIMENTALE IN VEICOLAZIONE E DIREZIONAMENTO DEI FARMACI

Different approaches to induce the self-assembly of PMPC-PDPA copolymer into vesicles for the delivery of plasmid DNA

Relatore

Ch.mo Prof.

GIUSEPPE BATTAGLIA

Candidato

MARCO BASILE

Matr. N78000413

Relatore interno

Ch.mo Prof.

GIUSEPPE DE ROSA

ANNO ACCADEMICO 2020/2021

To Claudia and Andrea

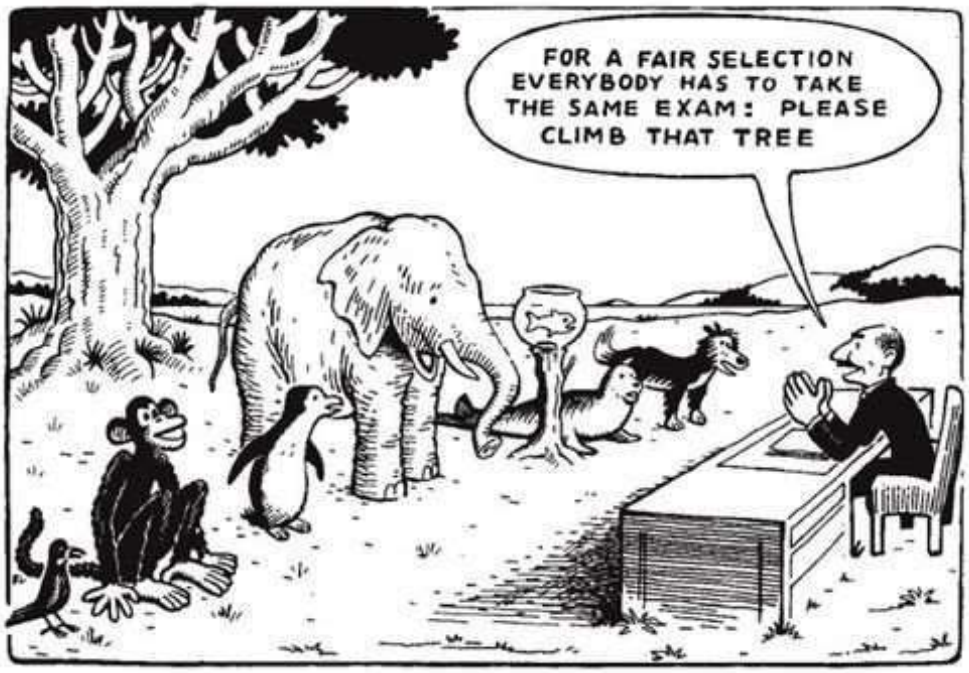

ACKNOWLEDGEMENT

First things first, I would like to acknowledge and give my warmest thank to prof. “Beppe” Battaglia and prof. Giuseppe De Rosa who made this work possible. Prof. G. De Rosa always showed to be supportive to clarify any doubts I had during my first period of apprenticeship in Naples. There, the supervising of Valeria Nele and Virginia Campani was fundamental in shaping me as a junior researcher and I believe that I cannot express my gratefulness enough with just a few words.

Likewise, in Spain, Beppe’s guidance and advice supported me through the entire project and hopefully towards new future goals in his team, where a friendship was created before a working relationship. I owe a deep sense of gratitude to Iris Batalha, who followed me step-by-step during the drafting of this thesis. My profound thankfulness also goes to Lara Aiassa and Cátia Lopes, who supported me in every step and moment of my internship at the Institute for Bioengineering of Barcelona (IBEC). I owe other acknowledgements to Gian, José, Claudia, Mohit, Daniel, Lorena, Anna, Barbara, Laura, and Matilde who have contributed to making this experience unforgettable. I would also thank anyone who helped me in this journey but does not appear in this picture.

INDEX

1. INTRODUZIONE

Secondo la *Food and Drug administration (FDA)*, la terapia genica si propone di alterare le proprietà biologiche delle cellule attraverso la modifica del genoma o modulando l'espressione di specifici geni. La terapia genica può essere attuata attraverso differenti approcci sfruttando gli acidi nucleici come farmaci terapeutici.

Plasmidi a DNA (*pDNAs*) e RNA messaggeri (mRNAs) spiccano tra gli acidi nucleici terapeutici in quanto l'informazione genetica contenuta nella loro sequenza può essere facilmente trascritta e tradotta dai sistemi cellulari endogeni. Questo ha dato la svolta nel campo dell'editing genomico basato sul sistema CRISPR-Cas, un meccanismo di immunità adattiva procariotica, che può essere ingegnerizzato per agire sul genoma umano o anche sul trascrittoma cellulare. Tuttavia, l'espressione del sistema CRISPR-Cas richiede l'adeguata veicolazione di *pDNAs* o *mRNAs*, ad oggi possibile con l'utilizzo di vettori, virali e non virali. Sebbene ampiamente diffusi, i vettori virali presentano limiti che facilmente possono essere superati dai corrispettivi vettori non virali.

I vettori non virali possono essere di natura biologica o sintetica, quest'ultimi divisi in organici e inorganici. Le nanoparticelle (NP) organiche sono tra le più promettenti e studiate. Sebbene differenti metodi siano stati predisposti per la loro formulazione, qui l'attenzione sarà rivolta a sistemi basati sul *self-assembly*. Rispettano tutte queste caratteristiche NP di natura lipidica o polimerica. Infatti, se disposte in un ambiente acquoso, la natura anfifilica delle molecole lipidiche o polimeriche permette la formazione di particolari strutture sovramolecolari. I processi che danno luogo a queste strutture possono seguire approcci definiti *top-down* o *bottom-up.*

2. MATERIALI E METODI

Il copolimero $PMPC_{25}$-$PDPA_{80}$ è stato utilizzato per la formulazione di polimerosomi, cioè vescicole chiuse, attraverso approcci di *top-down* o *bottom-up.* L'idratazione del film (approccio *top-down*) prevede, come prima fase, l'evaporazione del solvente organico di una soluzione polimerica organica

ad alta concentrazione (25 mg/mL) attraverso una stufa (T = 37°C, p = 200 millibar). Il film polimerico ottenuto è poi idratato con una soluzione salina sterile e posto sotto agitazione magnetica per indurre la vescicolazione. Il *solvent switch* (approccio *bottom-up*) invece prevede la sostituzione del solvente organico, in cui è solubilizzato il copolimero, con acqua. Questo processo avviene attraverso l'utilizzo di una *syringe pump*. Concentrazione del copolimero e velocità di iniezione del flusso d'acqua sono stati oggetti di studio. Cromatografia ad esclusione dimensionale (SEC), *Dynamic Light Scattering (DLS)* e microscopia a trasmissione di elettroni (*TEM*) sono state utilizzate per la purificazione e l'analisi dimensionale e morfologica dei campioni, rispettivamente.

3. RISULTATI E DISCUSSIONE

Nonostante l'idratazione del film polimerico si presenta una tecnica valida per la formulazione di polimerosomi, il tempo necessario per il suo completamento è di almeno sei settimane. Questo ha fatto sì che il *solvent switch* fosse preferito per i suoi tempi ridotti. In questo caso, è stato necessario modulare la concentrazione del copolimero e la velocità di iniezione del flusso d'acqua affinché polimerosomi della dimensione desiderata fossero ottenuti. La formulazione ottenuta alla concentrazione di copolimero di 10 mg/mL e alla velocità di iniezione di 0.5 uL/min è risultata ottimale per gli scopi preposti.

4. CONCLUSIONI

La veicolazione di acidi nucleici terapeutici risulta fondamentale affinché possano raggiungere intatti il sito bersaglio. I *pDNAs* rappresentano ad oggi il terzo vettore più usato, dopo gli *adenovirus* e *retrovirus*. L'applicazione dei *pDNAs* nell'ambito terapeutico necessita dell'uso di vettori non virali, capaci di preservare le molecole al suo interno. Pertanto, il progetto descritto in questa tesi mira alla formulazione di polimerosomi sufficientemente grandi e capaci di veicolare macromolecole come i *pDNAs*. Ulteriori studi saranno mirati alla verifica di tali presupposti.

LIST OF ABBREVIATIONS

AAV	Adeno-Associated Virus
AV	Adenovirus
ASO	Antisense Oligonucleotide
BBB	Blood-Brain Barrier
BEC	Brain Endothelial Cells
Cas	Caspase System
CNS	Central Nervous System
CRISPR	Clustered Regularly Interspaced Short Palindromic Repeats
crRNA	Crispr RNA
CAC	Critical Aggregation Concentration
D	Translational Diffusion Coefficient
DBD	DNA Binding Domains
DLS	Dynamic Light Scattering
DOPE	1,2-Dioleoyl-Snglycero-3-Phosphoethanolamine
DSPE	1,2-Distearoyl-Sn-Glycero-3-Phosphoethanolamine
EPR	Enhanced Permeability And Retention Effect
Epo	Erythropoietin
EMA	European Medicines Agency
FDA	Food And Drug Administration
HDR	Homology-Direct Repair
HER-2	Human Epidermal Growth Factor Receptor 2
HSC	Human Stem Cell
IL-10	Interleukin-10
LRP-1	LDL Receptor Related Protein 1
LV	Lentivirus
LCST	Lower Critical Solution Temperature
mRNA	Messenger RNA
miRNA	Micro-RNA
N_d	Degree Of Polymerisation
NC	Nanocarrier
NP	Nanoparticle
NHEJ	Nonhomologous End-Joining
p	Packing Factor
PC	Phosphatidylcholine
PE	Phosphatidylethanolamine
pDNA	Plasmid DNA
PDPA	Poly(2-(Diisopropylamino)Ethyl Methacrylate)
PMPC	Poly(2-(Methacryloyloxy)Ethyl Phosphorylcholine)
PLA	Poly(Lactic Acid)
POEGMA	Poly[Oligo(Ethylene Glycol) Methyl Methacrylate]
PEG	Polyethylene Glycol
PNIPAM	Poly-N(Isopropylacrylamide)
PAM	Protospacer Adjacent Motifs
R*	Minimum Critical Radius
ROS	Reactive Oxygen Species
rcf	Relative Centrifugal Force
siRNA	Short Interfering RNA
sgRNA	Single Guide RNA
SEC	Size Exclusion Chromatography
SST	Superselectivity Theory

SELEX	Systematic Evolution Of Ligands By Exponential Enrichment
T_m	Melting Temperature
TLR	Toll-Like Receptors
tracrRNA	*Trans*-Activating CRISPR RNA
TALEN	Transcription Activator-Like Effector Nucleases
TEM	Transmission Electron Microscopy
VEGF	Vascular Endothelial Growth Factor
ZFN	Zinc Finger-Nucleases

ABSTRACT

Since the first clinical approval in 1995 (Doxil®), nanomedicines have been marking the field of medicine by providing advanced healthcare approaches for the diagnosis and treatment of many pathologies. Inorganic and organic materials have been widely employed to design biocompatible nanocarriers (NCs) that can positively affect drug pharmacokinetics and toxicity. These materials have also been applied in gene therapy, supported by the rise of molecular biology in the second half of the twentieth century. In countless examples, nucleic acid therapeutics is determinant for treatment success [1, 2]. Up to date, with 3180 diverse gene therapies in clinical trials, plasmid DNA (pDNA) represents the third vector most used, behind adenovirus and retrovirus [3]. In the perspective of ascending the application of pDNAs in gene therapy, finding an adequate carrier seems an essential step.

In line with this goal, this work reports the preparation of polymersomes composed of a pH-sensitive poly(2-(methacryloyloxy)ethyl phosphorylcholine)-poly(2-(diisopropylamine)ethyl methacrylate) copolymer ($PMPC_{25}$-$PDPA_{80}$) via top-down and bottom-up methods. The process of self-assembly of $PMPC_{25}$-$PDPA_{80}$, induced by both film hydration and solvent switch approaches, will be discussed. Since the slow nature of the bending kinetics hampers the formation of closed vesicles, several parameters, such as copolymer concentration and injection rate, were optimised to obtain bigger polymersomes, avoiding the undesired formation of disk-like micelles. The end goal of this project is to optimise the preparation and physical properties (e.g., size) of $PMPC_{25}$-$PDPA_{80}$ polymersomes to deliver pDNAs to the brain. As stated by Battaglia [4], the PMPC chains can interact with SRB1 expressed on brain endothelial cells (BECs), favouring the crossing of the blood-brain barrier (BBB), giving added value to the use of this copolymer.

1. INTRODUCTION

1.1 - Gene therapy

According to the United States (U.S.) Food and Drug Administration (FDA), human gene therapy seeks to modify the genome or modulate the expression of a gene to alter the biological properties of living cells. This type of therapy can work by several mechanisms, as schematised in **Fig. 1**: i) replacing a disease-causing gene with a healthy copy of the gene; ii) inactivating a disease-causing gene that is not functioning properly; or iii) introducing a new or modified gene into the body to help treat diseases [5]. Several gene therapy medicines, so defined by European Medicines Agency (EMA) [6], have been approved since 1978 when for the first time it was revealed the therapeutic powerfulness of the antisense oligodeoxynucleotide (ASO) in inhibiting the Rous sarcoma virus 35S RNA via complementary binding [7].

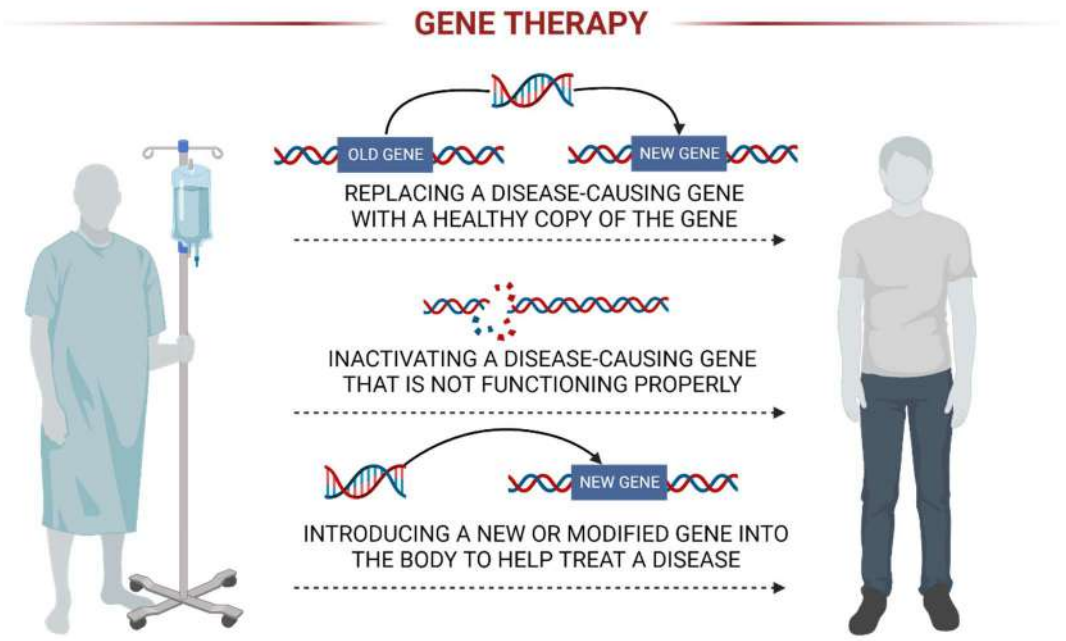

Figure 1. Three different approaches for gene therapy.

1.2 – Nucleic acid therapeutics

1.2.1 - ASOs

An ASO is a single strand of DNA that can interact with targeted messenger RNA (mRNA) by means of standard Watson–Crick base pairing, inducing its degradation or inhibition (**Fig. 2**). From their inception, three generations of ASOs have been developed to overcome their high susceptibility to nuclease enzymes, which leads to a short half-life and consequently incompatibility with therapeutic applications. The first two ASOs approved by the U.S. FDA are the fomivirsen in 1998, a first-generation ASO, and the mipomersen in 2013, a second-generation ASO, [8] followed by further six from 2016 to 2021 [9].

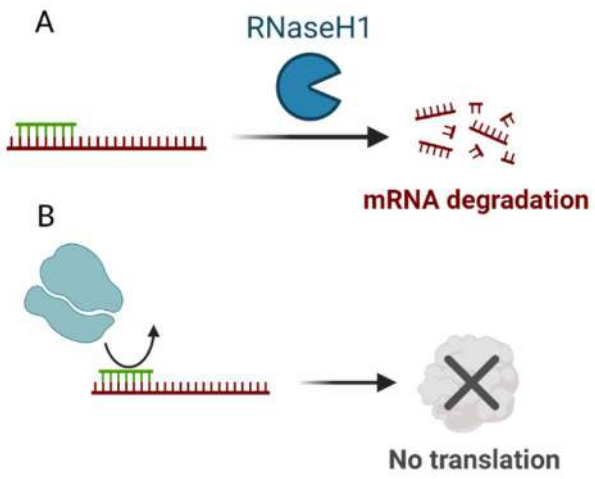

Figure 2. Possible mechanisms of action of antisense oligonucleotide: A) the ASO can recruit RNaseH1 to induce mRNA degradation. B) the steric inhibition of the ASO prevents the interaction between the mRNA and the ribosome.

1.2.2 – Aptamers

Aptamers are single-stranded, synthetic oligonucleotides that fold into 3-dimensional architectures capable of binding non-covalently to target molecules (e.g., proteins, peptides, carbohydrates, small molecules, toxins, and even live cells.) with affinities and specificities that are comparable to antibodies. Aptamers can be selected from large pools of random-sequence oligonucleotides through Systematic Evolution of Ligands by Exponential Enrichment (SELEX) [10, 11].

Unfortunately, the intrinsic physicochemical nature of aptamers implies an undesired pharmacokinetic profile, owing to nuclease degradation, rapid renal clearance, and non-specific immune response [12]. Nonetheless, aptamers modified and engineered into aptamer-drug conjugates [13] and aptamer-functionalised nanoparticle delivery systems [14] are widespread and under clinical investigation. In 2004, an anti-vascular endothelial growth factor (VEGF) RNA aptamer for treating ocular vascular disease was approved: the pegaptanib sodium, marketed as macugen [15].

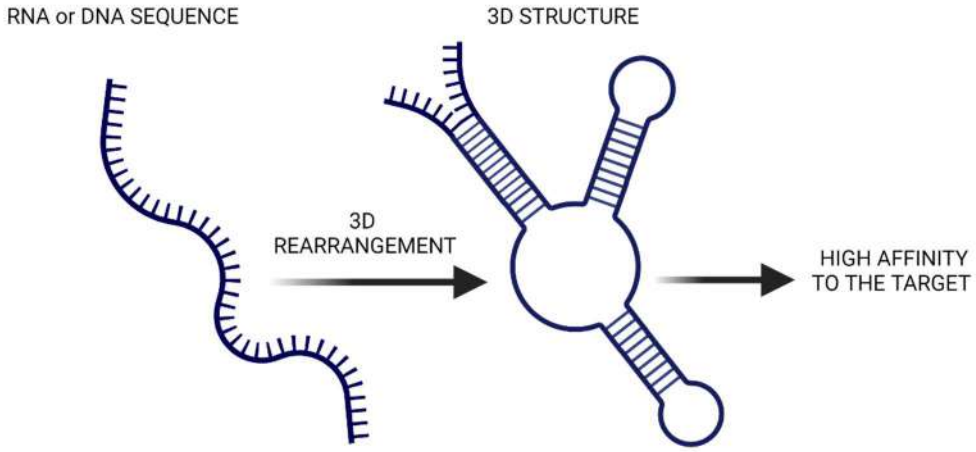

Figure 3. Aptamers structure: the 3D shape confers high affinity to the target.

1.2.3 – siRNAs and miRNAs

Short interfering RNAs (siRNAs) and microRNAs (miRNAs) are biologically classified as noncoding RNA since they merely act inside the RNA interference pathway (**Fig. 4**), as demonstrated for the first time by the Nobel prizes Andrew Fire and Craig C. Mello in 1998 [16]. After that, the correlation between interference RNAs' dysregulation and human diseases, such as cancer [17] and infection [18], has been established, and this has raised keen interest in using the same mechanisms to treat these pathologies. To bear witness of that: patisiran [19] and givosiran [20] are siRNAs already approved by FDA for the treatment of hereditary transthyretin-mediated

amyloidosis and acute hepatic porphyria, respectively. In contrast, miravirsen [21] is a miRNA in Phase II clinical trial for the treatment of hepatitis C.

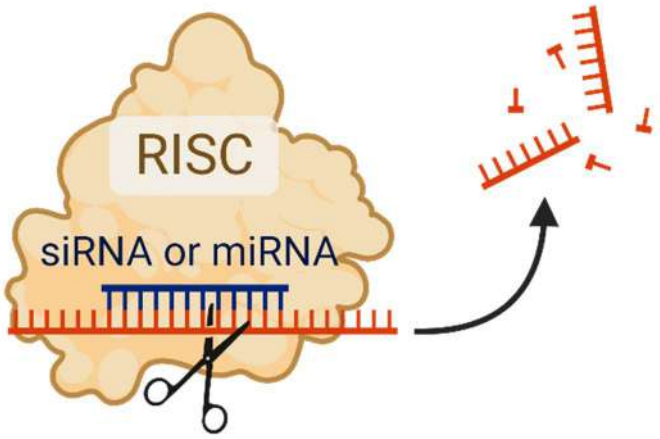

Figure 4. Interference pathway: siRNAs and miRNAs, after interacting with the mRNA (in red), can recruit the RNA-induced silencing complex (RISC) that will degrade the mRNA.

1.2.4 – pDNAs and mRNAs

In the last two decades, pDNAs and mRNAs have been drawing the attention of many since they can induce the expression of a protein of interest inside the cell (process displayed in **Fig. 5**). In 1990, Felgner and colleagues demonstrated how the protein expression of chloramphenicol acetyltransferase, luciferase, and ß-galactosidase was achievable by injecting naked pDNA or mRNA into mouse skeletal muscle *in vivo* [22]. From then on, pDNAs and mRNAs have been used for many potential therapeutical applications, from protein-replacement therapy to genome engineering and vaccines [23-25].

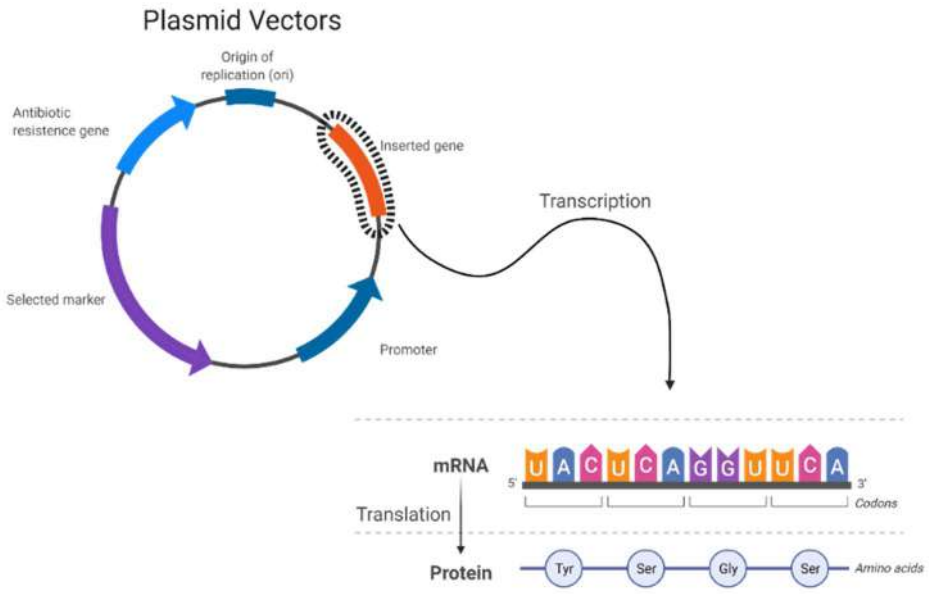

Figure 5. Transcription and translation in protein expression: from plasmid DNA to protein, through mRNA.

VEGF-A for myocardial infarction [26], interleukin-10 (IL-10) for inflammatory diseases or autoimmune myocarditis [27, 28], and erythropoietin (Epo) for lung disease [29] are just three examples of how the protein-replacement therapy can be realised with modified mRNAs. On the contrary, unmodified mRNAs have always shown intrinsic adjuvant activity and strong immune-stimulatory effect due to the interactions with Toll-like receptors (TLR3, TLR7, TLR8). This has made them suitable for the formulation of vaccines [30, 31]. Indeed, by combining all these features, it has been possible in less than one year to produce two mRNA Sars-CoV-2 vaccines, *e.g.*, mRNA-1273 (Moderna/NIAID/BARDA) [32] and Comirnaty, tozinameran (BioNTech/Pfizer) [33]. On the other hand, for a long time, the potency of DNA vaccines in eliciting a humoral response had been demonstrated feasible in preclinical studies [34, 35], but not in clinical trials [36, 37]. However, in 2021, the first DNA vaccine (ZyCoV-D) was approved in India [38].

1.2.5 – CRISPR-Cas

Without question, genome editing has revolutionised the biological world by providing a means to edit the genomes of living organisms, including humans, plants, animals, and microbes. In particular, the CRISPR-Cas system (i.e., clustered regularly interspaced short palindromic repeats (CRISPR) - caspase (Cas) system) [39], due to its versatility, flexibility, and adaptability, has become more widespread than previous programmable nuclease platforms, such as zinc finger-nucleases (ZFNs) and transcription activator-like effector nucleases (TALENs) (**Fig. 6**) [40, 41].

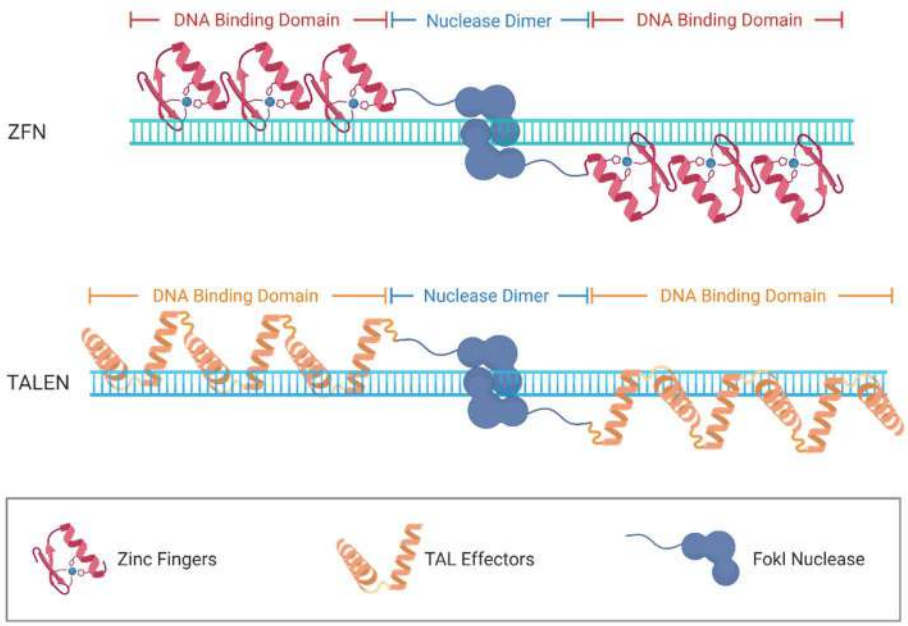

Figure 6. Mechanism of zinc finger-nuclease (ZFN) and transcription activator-like effector nuclease (TALEN). Both approaches demand proteic DNA Binding Domains (DBDs) to specifically recognise the targeted sequence, then cut by the nuclease. The main drawback of these techniques is the necessity to design, for any targeted sequence, a precise DBDs, which is more challenging and less precise than to synthesise the correct single guide RNA (sgRNA).

Briefly, the CRISPR-Cas system represents the adaptive immune mechanism developed by many bacteria and most archaea to protect themselves against bacteriophage infection and plasmid transfer. By now, six different CRISPR-Cas systems have been identified, and each one employs a unique set of Cas protein, among which the most known is the Cas9 endonuclease. This adaptive immunity is based on integrating exogenous DNA sequences in the CRISPR locus, which is transcribed into a long precursor CRISPR RNA (pre-crRNA) and then matured into the crRNA.

By interacting with the trans-activating CRISPR RNA (tracrRNA), the latter allows the engagement of the Cas9 endonuclease, which will leave the foreign DNA. The exogenous DNA is recognised by complementarity with the crRNA-tracrRNA complex (also known as guide RNA). There is also a built-in safety mechanism to ensure the Cas9 does not cut a random genome sequence. Short DNA sequences known as PAMs (*i.e.*, adjacent protospacer motifs) serve as tags and sit next to the target DNA sequences [42]. This entire bacterial machinery has been re-engineered to run as a programmable tool for genome editing [43] and transcriptional perturbation [44]. The mechanism is summarised in **Fig. 7**.

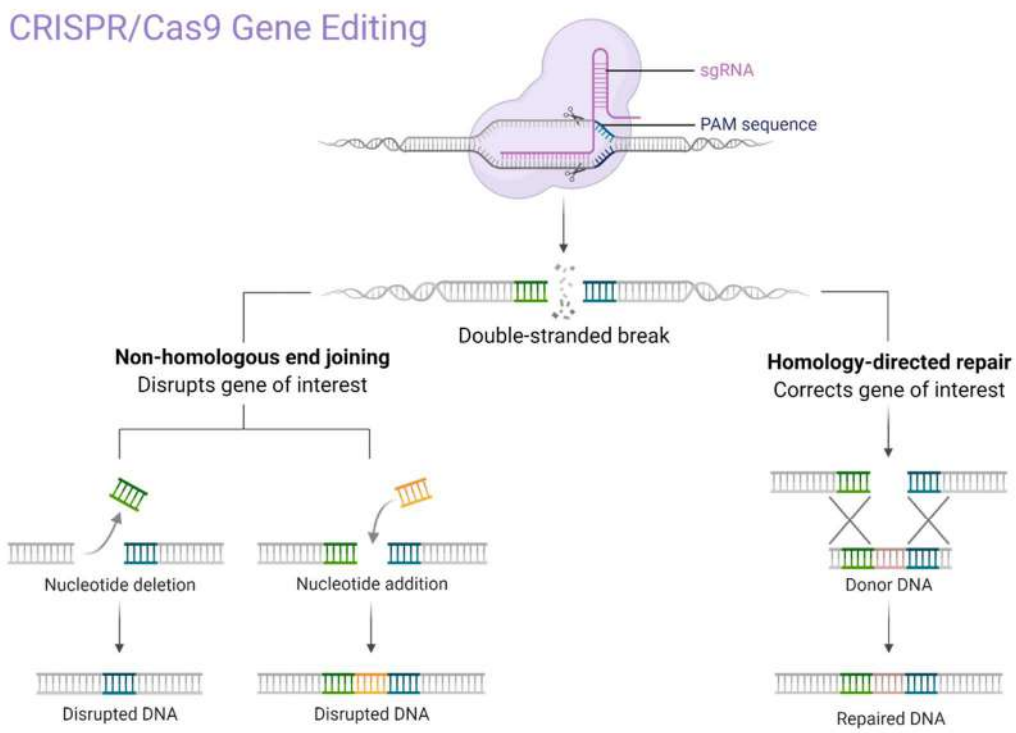

Figure 7. The re-engineered CRISPR/Cas9 mechanism allows to break a targeted DNA sequence in the genome. After the cut, the fate of the sequence can go through either the the nonhomologous end-joining (NHEJ) or the homology-direct repair (HDR) (the latter only whether a donor DNA template is provided). The NHEJ can be also used to degrade mRNAs, modulating the cell transcriptome.

In this type of therapy, pDNAs play a double role: i) in expressing within the cells the Cas protein and the single guide RNA (sgRNA), that is an engineered crRNA fused to the *tracr*RNA [45]; and ii) in providing a donor DNA template for enhancing the homology-direct repair (HDR), avoiding the nonhomologous end-joining (NHEJ) of the targeted sequence [39], and so aiming to precise genome editing, such as knock-in, deletion, correction or mutagenesis [42].

However, it is worth pointing out that the therapeutic efficacy of the CRISPR-Cas system, just as for the nucleic acid therapeutics mentioned in the above sections, is dependent on their ability to overcome a number of extracellular and intracellular biological barriers [46]. This necessity paved the way for a pioneering therapeutical approach: delivering delicate nucleic acids, such as those discussed above, while preserving their efficacy by using novel drug delivery systems. This field of research has been mainly focused on using two different types of carriers: viral and non-viral vectors.

1.3 – Viral and non-viral vectors

1.3.1 – Viral vectors

Viral vectors are composed of three major components: i) the protein capsid and the envelope, which both enclose the genetic material (DNA or RNA, single or double-stranded) and characterise the tropism of the virus; ii) the transgene of interest; and iii) the regulatory cassette, controlling the expression of the transgene. Altogether, these components allow the delivery, the transcription, and the translation of the transgene inside the desired cells by harnessing the physiological mechanism of infection of viruses [47].

In the last forty years, various attempts in gene delivery were made with at least five different viral vectors, all characterised by high delivery efficacy yet, regrettably, drawbacks. By now, just the

three shown in **Fig. 8** are the most used: lentivirus (LV), adenovirus (AV), and adeno-associated virus (AAV). The latter is less immunogenic and therefore preferred for therapeutical applications.

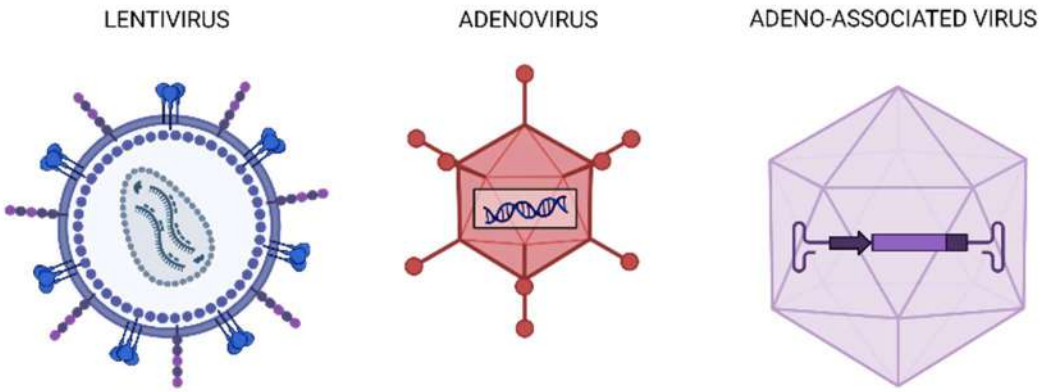

Figure 8. From left to right, the schematic representation of the lentivirus, adenovirus, and adeno-associated virus structure.

Nevertheless, previous studies have demonstrated that AAV vectors, employed for the delivery of CRISPR-Cas, can likely integrate into hotspots in mitochondrial DNA and in the spot termed AAVS1 on chromosome 19, thus representing a limit for their clinical use. Moreover, AVV carrying capacity is 4.7 kb, which makes it unable to deliver, for instance, the frequently used plasmid SpCas9, that is about 4.2 kb. Solutions have been found to remedy this issue, yet with shortcomings [48].

1.3.2 – Non-viral vectors

Concerning what was stated above, an alternative to viral vectors was needed, which led to the emergence of nanocarriers (NCs)/ nanoparticles (NPs) as auspicious vectors for gene and drug delivery. Typically, NCs have diameters ranging between 1 and 200 nanometres (nm) and possess diverse structures, shapes, and chemical compositions. Generally, the use of NCs can: i) enhance biodistribution, pharmacokinetics, stability, and solubility of the payload; ii) reduce the toxicity of

the cargo; and iii) provide sustained and targeted gene and drug delivery. [49]. NCs for gene delivery can be naturally occurring (biological) or synthetic (organic or inorganic).

i. Biological nanoparticles

Exosomes are biological NPs that originate from the vesiculation of endosomes. They are highly abundant in many biological fluids, such as serum, plasma, and cerebral spinal fluid, and act as biological nanoshuttles for delivering endogenous material between cells. Their small dimension, up to 200 nm in diameter, and capability of encapsulating any kind of biological material has drawn the attention of many as they can be engineered to carry nucleic acids. In 2011, Alvarez-Erviti *et al*.[50] demonstrated the successful delivery of siRNA to mice brain via systemic injection of targeted exosomes. Theoretically, the exosomes could result extremely compatible since they can be retrieved from stem cells of the patients, engineered, and then administered. Mathiyalagan P. and Sahoo S. developed a protocol about the generation of exosomes from human stem cells (HSCs) for the delivery of miRNA, which is summarised in **Fig. 9** [51]. Briefly, after HSCs cultivation in an appropriate medium, the cells are transfected with the miRNA of interest by using lipofectamine – a lipid-based transfection reagent. Subsequently, several steps of purification aim to remove cell debris, free miRNA, and eventual exosomes formed before the transfection. Then, in this case, a sucrose-based gradient ultracentrifugation is performed to obtain the desired exosomes: the density gradient allows to properly separate the low-density vesicles from the high-density vesicles.

However, different techniques have been studied to optimise the isolation of exosomes, as this is a critical step. Alternative approaches include combining ultrafiltration and size-exclusion chromatography (SEC) to isolate exosomes by fractionation, or using immunoaffinity chromatography for the specific binding of exosome membrane proteins [52].

The last step of the protocol developed by Mathiyalagan *et al.* was to test the exosomes transfection efficiency on human endothelial cells, quantifying the fluorescence of the dye linked to the miRNAs by confocal microscope.

Unfortunately, the same features that make exosomes attractive for drug delivery, also represent their pitfall. Indeed, exosomes are a reflection of the cell they originated from: both in terms of membrane elements and inner components, such as nucleic acids. Therefore, exosomes derived from mesenchymal stem cells have demonstrated to promote tumour growth *in vivo,* by enhancing the VEGF expression, an oncogene involved into angiogenesis of many cancers [53]. Moreover, exosomes loading methods suffer from poor efficiency of DNA transfer, low transfection efficiency and limit in payload size [54].

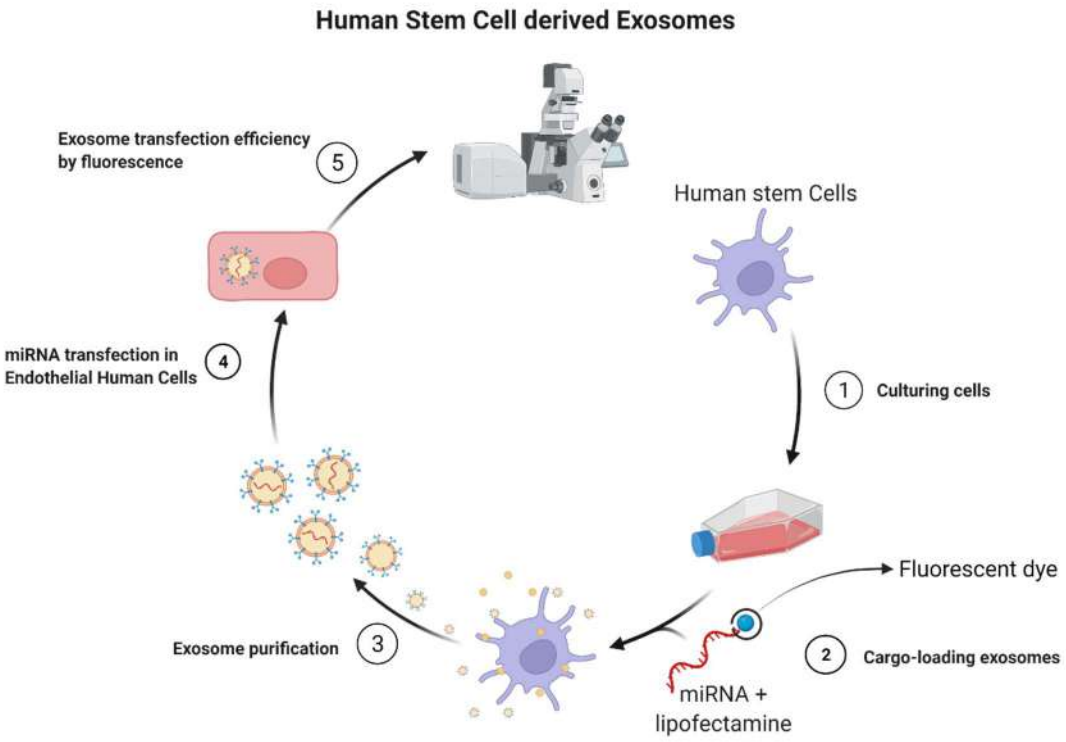

Figure 9. Outline of the Mathiyalagan *et al.* protocol [47]: how to obtain exosomes from HSCs and use them for the delivery of miRNA. 1) The human stem cells are firstly cultivated into the proper medium and then 2) transfected with the miRNA-lipofectamine complex. 3) Several steps of ultracentrifugation are done to isolate the exosomes from the cells. 4) Endothelial Human Cells are transfected with the exosomes and then 5) the miRNA is quantified by confocal microscope by fluorescence.

ii. Inorganic nanoparticles

Metal oxides (e.g., iron oxide, titanium dioxide, zinc oxide, cerium oxide, silicon dioxide), calcium phosphate, silver, and gold are the main materials involved in formulating inorganic NPs. The strict tuning of these materials has given the chance to formulate NPs which can be applied for diagnostic techniques, nanodrugs and delivery systems, and biomedical implants [55]. The broad use of NPs for the most diverse applications stems from the fact that materials have very different properties at the nanoscale dimension when compared to their bulk counterparts. Unique electronic, optical, magnetic, and mechanic proprieties can be obtained by tailoring and rationally designing the structure and composition of materials at the nanometre-scale.

Inorganic NPs are typically synthesised using chemical or physical methods. The chemical approach involves reducing metal ions to metal atoms in the presence of stabilisers, followed by the controlled aggregation of atoms. Physical methods, which frequently involve vapor deposition, depend on the principle of subdividing bulk metal precursors into NPs. Until now, chemical methods have prevailed over the physical approaches in mass-producing metal NPs, as the former provides a finer control of their size [56].

Amongst all the materials mentioned above, two have been standing out for the delivery of nucleic acids: calcium phosphate and gold. Although calcium phosphate NPs suffer from fast aggregation, this issue can be resolved by adding citrate at low concentration or polylysine, consequently leading to higher cargo transfection rates. Meanwhile, gold NPs (**Fig. 10**), with their tunable size and functionality, showed success in delivery of DNA and RNA, as well as peptides and proteins [55]. In 2009, Wijaya and colleague [57] reported the selective release of two distinct DNA oligonucleotides from two different gold nanorods via selective laser-induced melting of the nanorods. However, use of heavy metals as inorganic nanocarrier may result in the long-term health issues [58].

Figure 10. Different shapes of gold NPs.

iii. Organic nanoparticles

The most prominent and well-studied organic NPs for drug delivery are either lipid-based (e.g., lipid micelles, liposomes), or polymer-based (e.g., polymeric micelles, polymersomes). Although several methods of preparation of lipid and polymeric NPs have been elucidated, this thesis will focus on the self-assembly of amphiphilic structure in aqueous environment.

Lipid micelles are a supramolecular assembly, *i.e.,* a complex of amphiphilic building blocks/ molecules held together by non-covalent bonds. These building blocks are typically lipids – molecules characterised by a hydrophilic head and a hydrophobic tail. The hydrophilic head can be a polar or a charged group, while the hydrophobic tail is characterised by aliphatic chains. Fatty acids, phospholipids, and triglycerides are examples of lipids that possess one, two, or three aliphatic chains, respectively. These molecules have the ability to self-assemble in an aqueous environment, as the hydrophobic tails will tend to spontaneously gather in an inner core shielded by the hydrophilic moieties of the molecules, thus reducing the free energy of the system. The hydrophilic heads establish a network of hydrogen bonds in the aqueous environment, while the hydrophobic tails at the micelle core interact through hydrophobic interactions and Van der Waals forces [59]. However, this self-assembly process takes place only when the concentration of the amphiphile surpasses a threshold named ‘critical micelle concentration’ [60]. Until such

concentration is reached, the addition of amphiphile in an aqueous environment will only lead to the accumulation of the amphiphile at the water/air interface.

The amphiphilic nature of micelles has drawn the attention of many, since the loading of sparingly soluble drugs into the inner core could improve their bioavailability, reduce toxicity, and enhance drug permeation across physiological barriers [59]. Nevertheless, the instability of lipid micelles has been reported – they can easily disassemble or change their shape by varying experimental and post-experimental conditions, such as the temperature, pH, or amphiphile concentration. In addition to micelles, lipid amphiphilic molecules can arrange themselves by self-assembling into more complex structures, such as liposomes (**Fig. 11**).

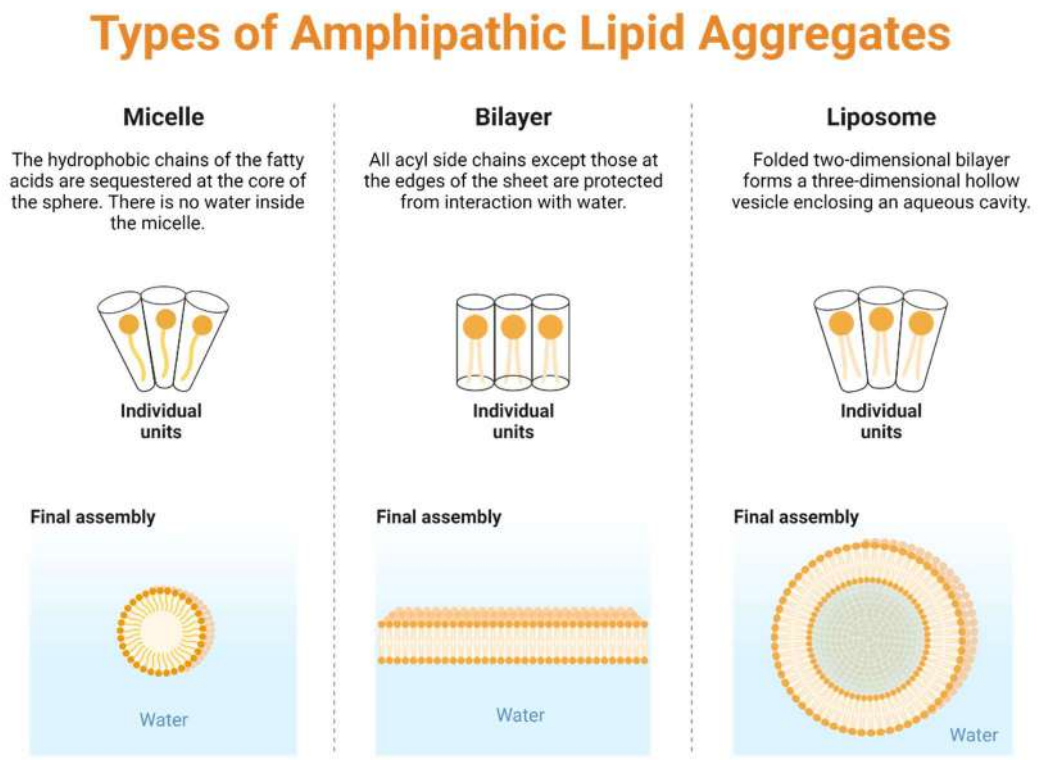

Figure 11. Lipidic amphiphile molecules can self-assemble into micelles, bilayers, and liposomes. The lipid structure can define the type of aggregate: fatty acids give rise to micelles, while phospholipids can first organise themselves in a bilayer and then fold into three-dimensional hollow vesicles, termed liposomes, as showed in the figure.

Liposomes are a colloidal suspension of self-assembling amphiphilic lipid molecules, such as phospholipids. Generally, phospholipids are organised into one or more lipid bilayers

(lamellae), surrounding an internal aqueous core with the polar head groups oriented to the inner and outer aqueous phase. Single-bilayer liposomes are classified as unilamellar, whilst multilamellar liposomes have an onion-like structure with more concentric bilayers. Mainly, the lamellarity, the size, and the encapsulation efficiency of liposomes depend on the production methods: the film hydration, followed by the extrusion, being the most common (**Fig. 12**).

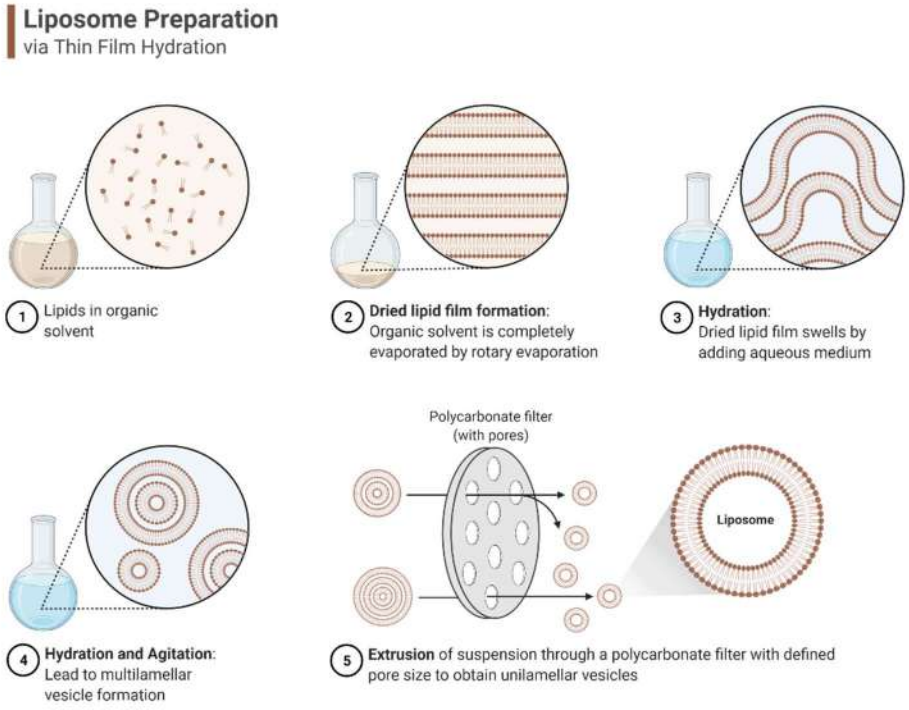

Figure 12. Liposome preparation via thin film hydration.

Liposomes are typically composed of glycerophospholipids [61]: a glycerol molecule bound to a phosphate group and to two fatty acid chains, saturated or unsaturated. The phosphate group usually binds to an organic group, the most common being choline (phosphatidylcholine; PC) and ethanolamine (phosphatidylethanolamine; PE). Since the safety, stability, and therapeutic efficacy of liposomes are defined by their phospholipids' composition, synthetic versions of these are widespread, such as 1,2-dioleoyl-snglycero-3-phosphoethanolamine (DOPE), and 1,2-distearoyl-sn-glycero-3-phosphoethanolamine

(DSPE). Likewise, to further enhance the *in vivo* stability of liposomes, cholesterol is often incorporated in the lipid bilayer, enhancing the membrane stiffness, and reducing its permeability. In addition, phospholipids can also be further conjugated to polymers, *e.g.*, polyethylene glycol (PEG), aiming to increase the half-life from few minutes to several hours by reducing the renal clearance and avoiding the reticuloendothelial system. These types of liposomes are coined stealth or PEGylated liposomes. Unsurprisingly, Moderna and Pfizer-BioNtech have relied on this type of PEGylated liposomes to deliver their mRNA Covid-19 vaccines [61]. However, it is worth mentioning that PEG has been reported to cause some levels of immunogenicity, and therefore it is paramount to keep tight pharmacovigilance protocols [62].

Unfortunately, other parameters hinder the widespread use of liposomes in drug delivery. For instance, liposomes can be obtained only if the temperature at which the self-assembling occurs is above the melting temperature (T_m) of the phospholipid components. The T_m represents the temperature at which the amphiphile's physical state changes from an ordered gel phase to a disordered liquid crystalline phase, which allows the arrangement of the phospholipids into liposomes. As a consequence, temperature-sensitive drugs (e.g., proteins and nucleic acids) cannot be encapsulated in liposomes. Moreover, phospholipids are susceptible to hydrolysation by ubiquitous esterase. A major shortcoming of phospholipids presenting unsaturated aliphatic chains, is their proneness to be oxidated by reactive oxygen species (ROS), thus weakening the stability of bilayer. These factors, allied to the low molecular weight of phospholipids, are translated into a tendency for leakiness and consequent off-target release of incorporated drugs. Indeed, the poor retention efficiency of cargo during the encapsulation process within liposomes is a commonly reported problem [63].

Polymersomes arose as a potential and promising alternative to solve some of the issues related to liposomes. Polymersomes are NCs made of amphiphilic block copolymers which self-assemble in water into closed vesicles. The molecular weight of the polymeric building blocks is typically higher than phospholipids, which guarantees enhanced stiffness. Furthermore, polymersomes are highly stable structures owing to the unique entanglement which takes place amongst the hydrophobic moieties of the copolymers. Such entanglement creates a robust membrane; therefore, allowing superior retaining efficiency of cargo. In addition to providing the system a durable lifespan, the block copolymers can also be adapted to accomplish a tunable release of the cargo [63].

Such polymersomes can be sensitive to different kinds of stimuli – they can be hydrolysable, thermo-responsive, photo-responsive, and/or pH-responsive. According to Hu *et al.*, poly-N(isopropylacrylamide) (PNIPAM) is the most reported thermo-responsive copolymer, with a lower critical solution temperature (LCST) of 32°C (i.e., the temperature at which it disassembles). For instance, a diblock copolymer PEO-b-PNIPAM (LCTS of 36°C) can self-assemble into vesicles above the physiological temperature (37°C), encapsulating hydrophilic drugs into the aqueous lumen or hydrophobic molecules in the bilayer, for then releasing them when the temperature decreases [64].

Light-responsive polymersomes are based on the use of copolymers whose cargo release profile is affected by light wavelength, intensity, or exposure time. The light sensibility depends on the photo-responsive moiety. For example, azobenzene can switch from *trans*-to-*cis* isomer, inducing the deformation of the vesicles from a spherical shape to an earlike shape, which triggers the disruption of the membrane and release of the cargo [64]. Another approach to control the cargo release is by using hydrolysable polymers containing polyester, polycarbonate or polyacetal linkages. The vesicles disassembly, induced by the

hydrolysis of the above-mentioned bonds, can range from hours to month as demonstrated by Kumar *et al*., which studied polymersomes with different PEG-to-PLA ratios [65].

The last subject of discussion are pH-sensitive polymersomes. They can be formulated with hydrolytic acid cleavable polymers, or the most common building blocks composed of ionisable groups such as polyacid (e.g., carboxylic or sulfonic acids) or polybasic (e.g., amines). The solubility of these polymers depends on the pH – when the ionisable block is charged, the polymer turns out to be water-soluble. This pH-responsiveness can be harnessed to induce cargo release: the ionisation of the polymer, induced by the change of pH, increases its water-solubility and consequent disassembly. A pH-sensitive copolymer well-studied by Battaglia *et al.* [66] is the PMPC-PDPA. As shown in **Fig. 13**, the PMPC-PDPA owes its pH responsiveness to the PDPA chains, which become ionised when the pH goes below its pK_a.

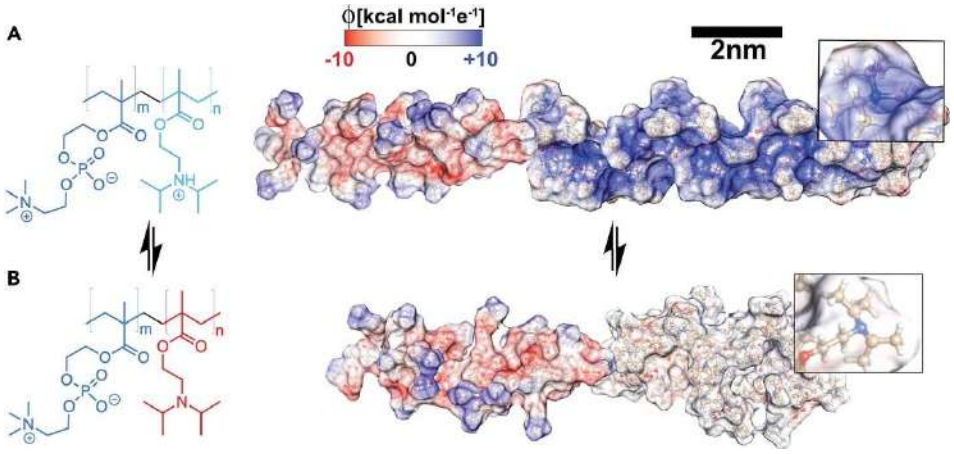

Figure 13. $PMPC_{25}$-$PDPA_{72}$ with the PDPA amine groups protonated (A) and deprotonated (B). Positive charged zones are depicted in blue, whereas negative charged zones are depicted in red (Battaglia *et al.* [66]).

As demonstrated by Battaglia and co-workers, since the $PMPC_{25}$-$PDPA_{72}$ pK_a is around 6.8 [66], the disassembly of the polymersomes occurs immediately after their cellular internalisation, within the early endosomes, which are slightly acidic. This disassembly

triggers the release of its pH-sensitive building blocks, and the correlated rise of the osmotic pressure elicits the lysis or the swelling of early endosome membrane (**Fig. 14**). The cargo can therefore escape the endosome and diffuse into the cell cytosol, escaping from lysosomal degradation [65].

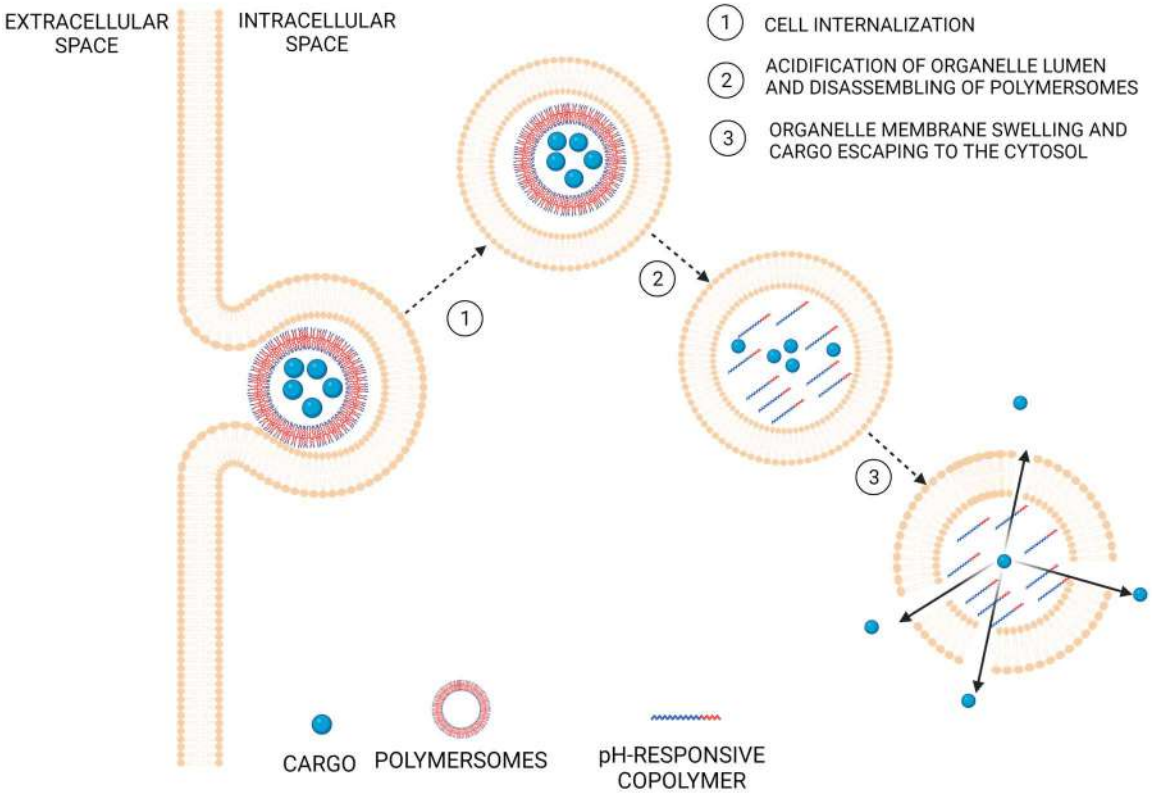

Figure 14. Mechanism of pH-sensitive polymersomes. As soon as the polymersomes enter endosomes, they will experience acidic pH. Since the endosomal pH is lower than the copolymer pK_a, the polymersomes disassemble. Then, the high osmotic pressure generates the swelling of the membrane with the consequent release of the cargo into the cell cytosol.

For a highly efficient encapsulation and delivery of hydrophilic compounds (e.g., nucleic acids), it is paramount to use suitable polymeric NPs with an inner aqueous compartment. Polymersomes fulfil this feature, yet the vesiculation process is affected by both methods of preparation and physical rearrangement of amphiphiles in water, described by the critical packing factor (defined below, Eq. 1).

Techniques such as electroformation, lithography, microfluidics, and double emulsion are widely used to form micrometer-sized polymersomes, which can be harnessed to study, for

instance, membrane confined processes. Therefore, such approaches will not be furtherly discussed herein [65]. On the other hand, methods of preparation for nanoscale polymersomes involve top-down or bottom-up methods.

The top-down approach consists of solvent free methods involving the hydration of a dry block copolymer film. The driving force of the polymersomes formation lies in the concentration gradients between the copolymer film, diffusing in water, and the water front, diffusing in the copolymer [67]. When the water interpenetrates copolymer molecules in the dry film, lyotropic lamellar structures form. Then, more water diffuses into lyotropic structures, producing the swelling and the unbinding of lamellar phases into sponge phase structures. Furthering the dilution of the copolymer, the sponge phase structures turn into hexagonal-packed vesicles, at the copolymer concentration of 1% w/w, and then into dispersed vesicles (polymersomes) at 0.5% w/w (**Fig. 15**) [68, 69].

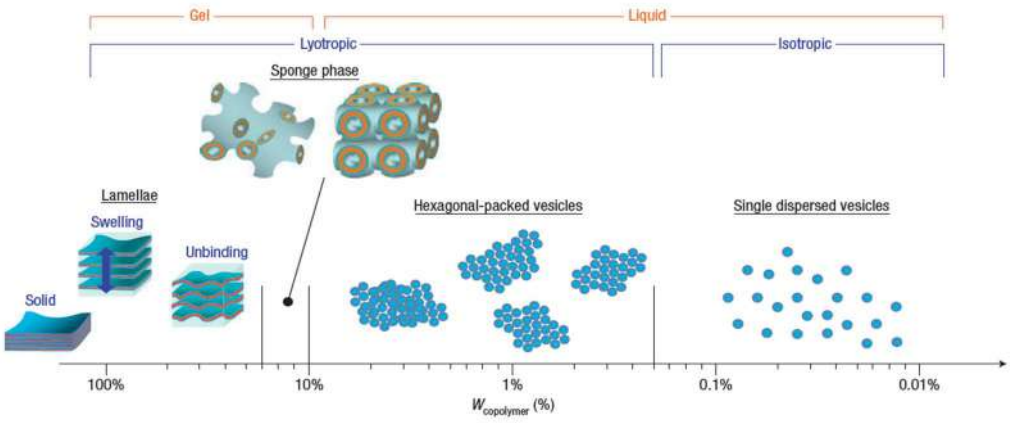

Figure 15. The phase diagram of copolymer in water. The transition from solid bulk copolymer to single dispersed vesicles (*e.g.,* polymersomes) occurs when the copolymer concentration in water decreases (Battaglia *et al.* [69]).

The transition from lamellae to sponge phase is unaltered by the molecular weight of the amphiphile. On the other hand, the evolution of sponge structures into dispersed vesicles depends on the size of the amphiphilic block of the copolymer. Therefore, small copolymers give rise to dispersed vesicles at quite high concentration, whilst high

molecular weight copolymers initially form vesicular gel clusters, which eventually break up into dispersed vesicles. Moreover, the copolymer molecular weight also affects the transition kinetics from one phase to the other. Indeed, in comparison with small amphiphiles, macromolecular copolymers give rise to structures with non-ergodic nature and kinetically entrapped [67]. This means no exchange occurs between polymersomes and the bulk solution, indicating a critical aggregation concentration (CAC) close to zero. The latter represents the concentration at which the amphiphile starts to self-assemble into well-known structures, such as closed vesicles.

Since the direct hydration of copolymer film is an approach limited only to copolymers with relatively high flexibility, the bottom-up method provides a valid alternative for glassy and crystalline copolymers, uncapable to self-assemble due to unfavoured kinetics. Indeed, in the solvent switch method, the copolymer is initially fully solubilised and molecularly dispersed in organic solution, and the vesicle formation is achieved by gradually exchanging the organic solvent with water. The vesiculation process occurs thanks to the increase of the hydrophobe-water interfacial tension triggered by the injection of water into the organic environment [67]. Since the hydrophobic moieties are prone to interact with each other when in water, the free energy of the system decreases as the copolymers self-assemble [70]. The way in which the copolymers self-assemble defines different structures: spherical micelles, cylindric micelles, or membrane-like structures. Such structures can be described by a dimensionless parameter, that is the critical packing factor. The amphiphile critical packing factor (p) can be described as:

$$p = \frac{v}{a_0\, d} \qquad \textit{Eq. 1}$$

Where v is the volume, d is the length of the hydrophobic block, and a_0 is the optimal area of hydrophobic block at the interface between the hydrophobic and hydrophilic block. As a general rule, spherical micelles are formed when $p \leq 1/3$, cylindrical micelles are formed

if 1⁄3 < $p \leq$ 1⁄2, and membranes arise when 1⁄2 < $p \leq 1$ [71, 72]. Moreover, the dimensionless p is linearly proportional to the hydrophobic/hydrophilic ratio, which in turn defines the optimal surface area (a_0) at the interface between the hydrophobic and hydrophilic blocks (**Fig. 16**).

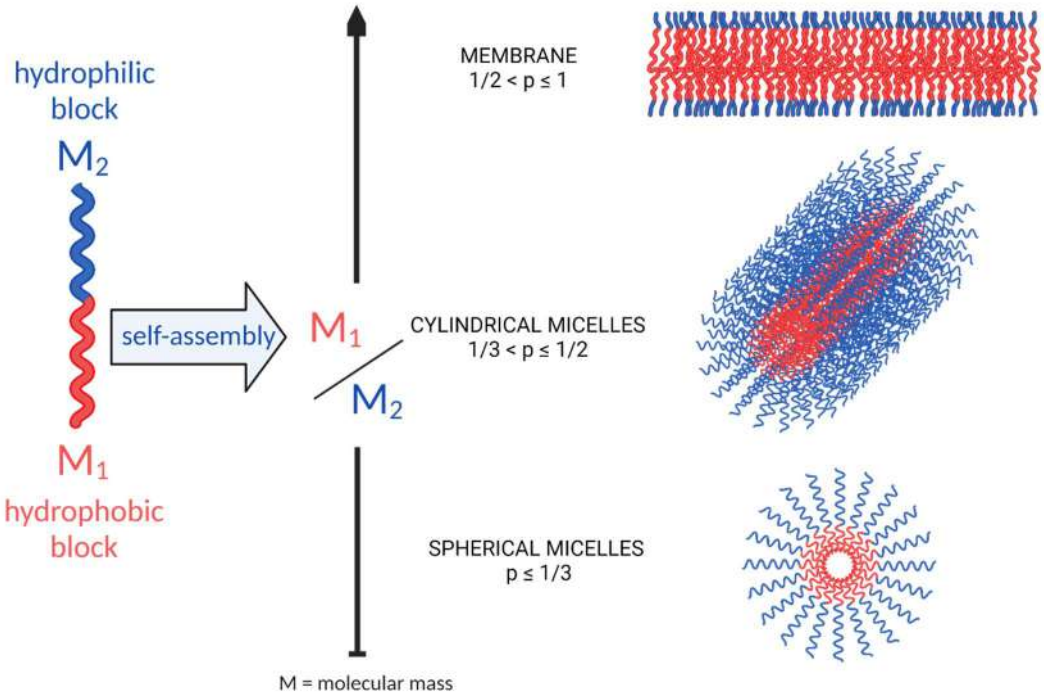

Figure 16. Schematic representation of the potential supramolecular structures achievable from the self-assembling of macromolecular amphiphiles. Spherical micelles occurs when the packing factor (p) ranges between 0 and 1/3, while cylindrical micelles form with 1/3 < $p \leq$ 1/3. Membranes arise when 1⁄2 < $p \leq 1$.

Similar to lipid micelles, spherical polymeric micelles are self-contained assemblies, with a compact inner hydrophobic core completely surrounded by the hydrophilic blocks. In 2018, Shen *et al*. demonstrated the efficiency of pH-responsive polymeric micelles as NCs to deliver oligonucleotides of different lengths to breast cancer cells. The polymeric micelles, compared to the free oligonucleotides, proved to protect the oligonucleotides from degradation with consequent higher cytotoxic effect on tumoral cells overexpressing the human epidermal growth factor receptor 2 (HER2) [73].

Differently from spherical micelles, cylindric micelles and membranes are supramolecular structures which expose part of the hydrophobic core towards the aqueous environment. From a theoretical point of view, infinitely long cylindric micelle and infinitely large membrane represent the most stable condition, though impractical. Thereby, as the contact between the hydrophobic part and the water is thermodynamically unfavoured, a certain level of frustration and consequently curvature in that structure is necessary. Whether the molecular frustration is limited to the outer part of the cylindrical micelles and membranes, respectively, wormlike structures and disk-like micelles occur. When the molecular frustration is shared amongst all the molecules, the cylindrical micelles bend into toroidal micelles, while membranes close into vesicles, *i.e.*, polymersomes [66].

It is fundamental to refer that the degree of polymerisation of the hydrophobic chain in copolymers determines the thickness of membrane in polymersomes and the radius of disk-like micelles. As demonstrated by many [71, 72, 74], the membrane thickness of polymersomes is associated to the number of units (N) characterising the hydrophobic block by the following rule $thickness \approx N^{2/3}$, whilst for the radius of disk-like micelles the relationship is $radius \approx N^{1/3}$. Thereby, by knowing the membrane thickness and the length of the hydrophilic block, it is possible to evaluate the minimum critical radius at which the disk-like micelles start bending and enclosing into vesicles, *i.e.*, polymersomes (**Fig. 17**).

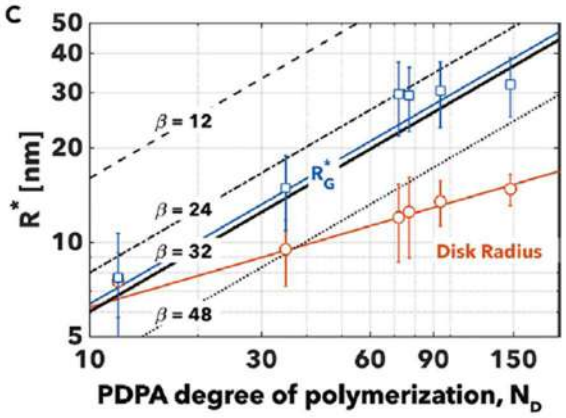

Figure 17. Correlations of the PDPA degree of polymerisation (N_D) with minimum critical radius (R*) at which the disk-like micelles start bending. The pressure distribution across the membrane is summarised by the constant β, which for polymersomes results to be equal to 32. β = 48 corresponds to uncoupled membrane free to slide on each other, while β = 12 for a coupled membrane with a pressure distributed uniformly across the membrane (Battaglia *et al*. [66]).

The vesiculation process is controlled by two kinetics: the nucleation and the bending. The nucleation process is the fastest one and consists of an initial assembly of the amphiphile unimers in disk-like micelle structures. Since the disk-like micelles growing depends on the integration of unimers into the membrane of pre-formed assemblies, the bending kinetics is the slowest. Therefore, processes based on fast kinetics demonstrated to produce more disk-like micelles than polymersomes (**Fig. 18**).

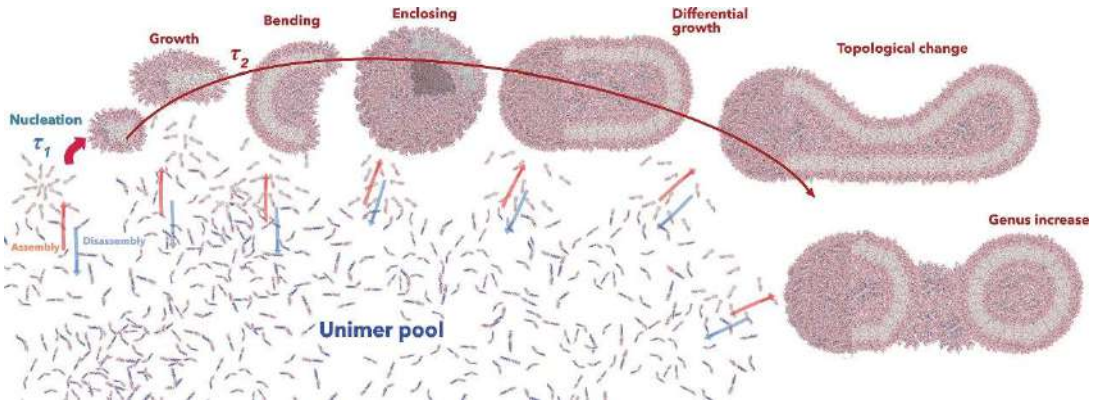

Figure 18. Mechanism of polymersomes formation and topological changes. The unimer pool depicts free copolymers in solution, which can assemble (red line) or disassemble (blue line). The kinetics of the nucleation process is faster than the bending one since the latter requires the diffusion of unimers into pre-formed membranes. However, if the unimers continue to diffuse into the membrane, topological change occurs (Battaglia *et al.* [66]).

1.4 – Passive and active targeting

NPs can reach their desired biological targets through passive or active targeting. Indeed, for some diseases, such as cancer, passive targeting is attained due to the spontaneous accumulation of nanoparticles in the diseased tissue as a result of poor lymphatic drainage and leaky vasculature (**Fig. 19**). This effect is known by the enhanced permeability and retention effect (EPR).

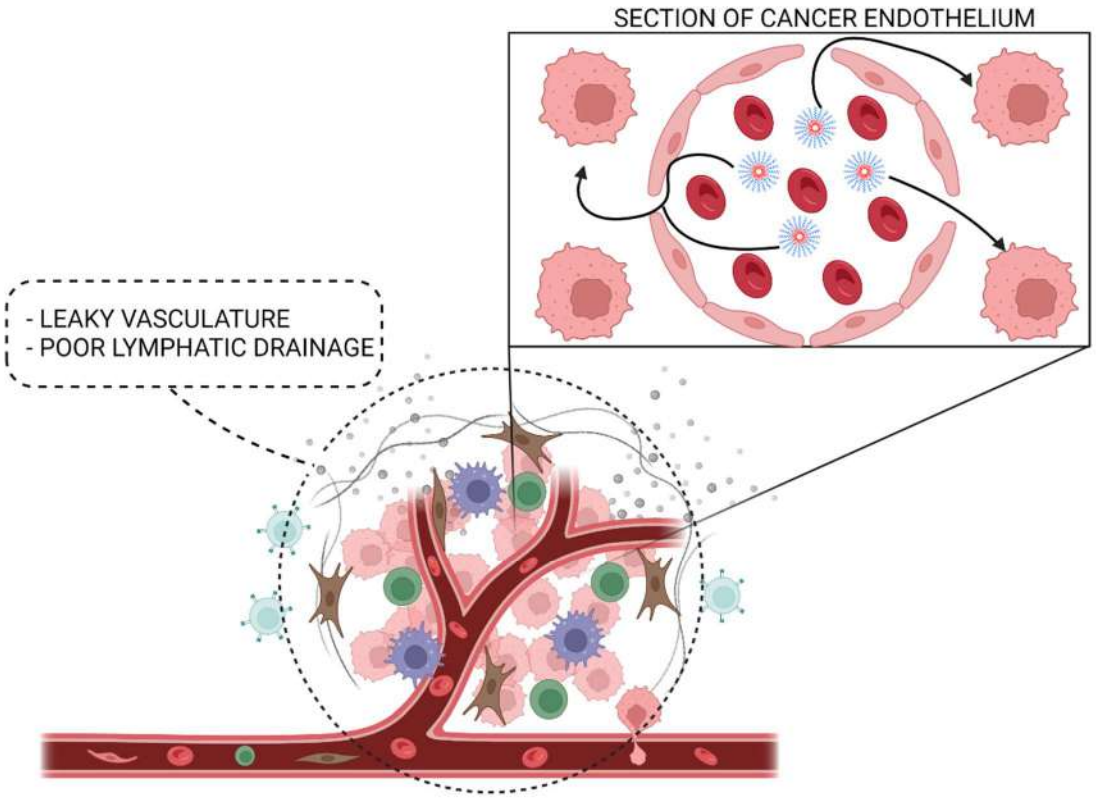

Figure 19. Extravasation of NPs from a blood vessel to the cancer stroma through the leaks of the cancer endothelium.

NPs can extravasate from the blood vessels to the inner part of the tumour through the more permeable pathologic vasculature, while their accumulation into tumour stroma is fostered by the lack of lymphatic drainage [75]. As demonstrated by Ngoune *et al.* [76] and Cabral *et al.* [77], a strict correlation exists between the NPs diameter, up to 100nm, and their capability to harness the EPR effect in tumours. Even though the EPR effect is deemed the "golden principle" in the passive targeting field, the concept is gradually becoming more controversial as the percentage of failures

in clinical trials of EPR-based delivery of NPs is increasing, perhaps owing to the broad heterogeneity of the studied tumours [78, 79]. Aiming to augment their therapeutical efficacy, NPs' surface can be functionalised with ligands that promote active targeting of specific tissues and subsequent receptor-mediated nanoparticle internalisation. This type of targeting can be fundamental to reach inaccessible areas, such as the central nervous system (CNS), where the BBB serves as an essential protection mechanism that selectively allows individual molecules such as small lipid-soluble molecules to pass through the capillary endothelial membrane while limiting the passage of pathogens, toxins, and most therapeutic drugs. Thus, harnessing existent transporter molecules, such as the one mediated by the low-density lipoprotein receptor-related protein 1 (LRP-1), using targeted nanotherapeutics might be a clever way to overcome the BBB (**Fig. 20**).

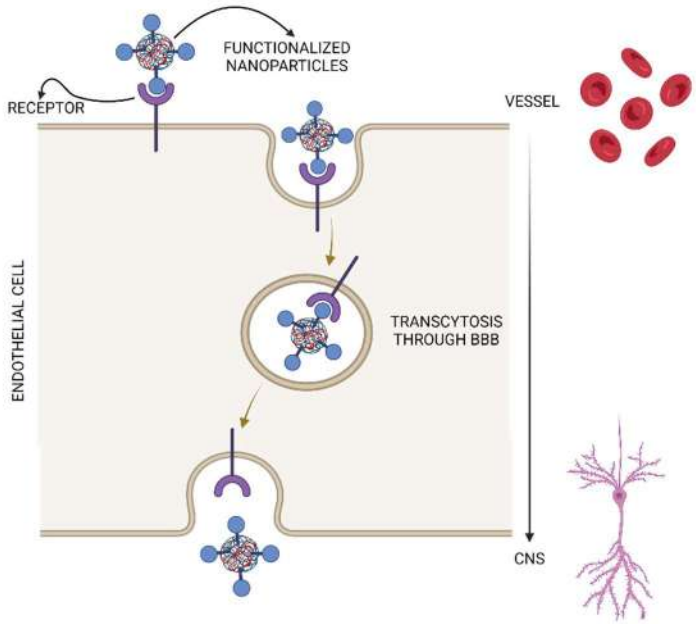

Figure 20. Functionalised NPs passing through the BBB by receptor-mediated transcytosis.

Therefore, several ligands, such as antibodies, other proteins, and peptides, have been utilised to target specific receptors. An interesting approach is to play with both the affinity and avidity of multivalent NPs. This type of phenotypic targeting is discussed by Battaglia *et al.* in "*On the design*

of precision nanomedicines" [4], wherein the general concept of superselectivity theory (SST) [80] is combined with principles from soft matter and polymer physics.

The SST posits that NPs decorated by low-affinity ligands can selectively bind cells as function of the receptor density non-linearly. Provided the single bond is sufficiently weak, only when several bonds are formed the NP binds to the cells effectively, enabling targeting only cells that overexpress the targeted receptors. Such a concept however has been considered theoretical for several years and only recently adapted to nanomedicine applications. Battaglia *et al.* combined multivalent interactions with repulsive steric potentials arising from hydrophilic polymers such PEG, effectively creating a combined interaction whose magnitude fulfils the SST requirements. This was experimentally confirmed by the use of amphiphilic poly[oligo(ethylene glycol) methyl methacrylate]-poly(2-(diisopropylamine)ethyl methacrylate) (POEGMA-PDPA) polymersomes double functionalised with angiopep-2 and PMPC chains, which respectively target LRP-1 and SRB-1 receptors on BECs for the targeted delivery of medicines to the brain [4].

2. MATERIALS AND METHODS

2.1 – Materials

$PMPC_{25}$-$PDPA_{80}$ copolymers were provided by SomaServe Ltd UK. Chloroform, methanol, and tetrahydrofuran were purchased from Merck Life Science SLU. All solvents were ≥ 99% pure. The 1kDa membrane used for the nanoparticle dialysis was acquired from Fisher Scientific. PBS tablets and sterile GIBCO PBS pH 7.4 (1×) were supplied by Life Technologies, SA (Thermo Fisher). Sepharose™ 4B columns for size-exclusion chromatography (SEC) were acquired from Merck Life Science SLU. 96-well plates with transparent bottom were purchased from Greiner Bio-One España, S.A.U. (PR2565). Phosphotungstic acid hydrate (PTA) used to stain samples for transmission electron microscopy (TEM) was acquired from Merck Life Science SLU. The TEM grid of carbon film on copper was acquired from EM Resolution. For all the experiments deionised and filtered (0.22 μm) water was used. *Parque Científico de Barcelona* (PCB) provided sterile water.

2.2 – Methods

2.2.1 – Film hydration (top-down approach)

25 mg of $PMPC_{25}$-$PDPA_{80}$ copolymer was weighed and then solubilised in 1 mL of chloroform and methanol in 2:1 volume ratio. The chloroform was added first and then the methanol to reach the final volume. The vial with the solubilised copolymer was covered with sterile Whatman® filter paper to allow solvent evaporation, while keeping the environment as sterile as possible. The vial was placed into the vacuum chamber "Vaciotem-TV" of JB-Selecta at 37°C and 200 millibar until a dried film was obtained, as showed in **Fig. 21**.

Figure 21. Copolymer film after solvent evaporation in vacuum chamber.

Then, under sterile conditions, the copolymer film was hydrated with 5 mL of sterile GIBCO PBS 1X to reach a copolymer concentration of 5 mg/mL. Immediately after hydration, the suspension was placed under stirring at 800 rpm for six weeks on multipoint magnetic stirring IKA® RT 5. The set-up is showed in **Fig. 22**. After six weeks, the sample was purified as follows: sonicated using a XUB5 Digital Ultrasonic Bath (Grant Instruments) for 15 minutes in ice, to avoid the heating of the sample, and then centrifuged for 10 minutes (set on 9 minutes up and 1 minute down) at 1000 Relative Centrifugal Force (rcf) using a Centrifuge 5810 R (Eppendorf). The supernatant was collected and purified by size exclusion chromatography (SEC).

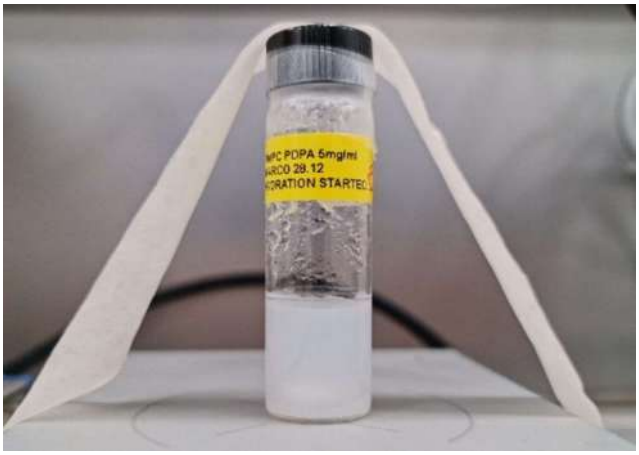

Figure 22. Set-up after the hydration of the copolymer film.

2.2.2 – Solvent switch (bottom-up approach)

The $PMPC_{25}$-$PDPA_{80}$ copolymer was weighed and then solubilised in a mixture of methanol and tetrahydrofuran in a 3:1 volume ratio. Three different concentrations were tested: 2 mg/mL, 10 mg/mL, and 20 mg/mL. From then on, everything was carried out under sterile conditions. A NE-1000 programmable single syringe pump (New Era Pump Systems Inc) was used to inject sterile water into the copolymer solution, always kept under stirring at 400 rpm on a big squid magnetic stirrer of IKA®. The syringe parameters were set up so that the volume injected was 2.3 times the volume of copolymer solution, and six different flow rates were tested: 0.5 µL/min, 2 µL/min, 5 µL/min, 25 µL/min, 50 µL/min, 100 µL/min. The suspension was collected and placed inside a 1 kDa dialysis membrane when the injection was over. This dialysis membrane had been in ethanol 24 hours and washed with sterile water before use. The dialysis membrane with the sample was kept in a beaker with 700 mL of sterile water under constant stirring for the first hour and then changed to sterile PBS 1X. The sterile PBS 1X was changed every 12 hours for at least 48 hours. After dialysis, the sample was purified as follows: sonicated using a XUB5 Digital Ultrasonic Bath (Grant Instruments) for 5 minutes in ice to avoid the heating of the sample, and then centrifuged for 10 minutes (set on 9 minutes up and 1 minute down) at 1000 rcf in a Centrifuge 5810 R (Eppendorf). The supernatant was collected and then purified by SEC. After this purification and at every previous step of the formulation process, the samples were analysed by dynamic light scattering (DLS) to determine the hydrodynamic size distribution of the samples. In addition, to study particle morphology, the sample was analysed by transmission electron microscopy (TEM). **Fig. 23** shows the set-up of the injection phase.

Figure 23. Set-up of solvent-switch method.

2.2.3 – Size Exclusion Chromatography (SEC)

SEC is a technique that allows separating molecules according to their size. The stationary phase consists of spherical porous particles with a carefully controlled pore size, through which molecules diffuse pushed by a mobile phase. These pores can be depressions on the surface or channels through the beads. Smaller molecules are trapped into the stationary phase pore system and can go through a larger volume (the sum of the entire pore volume and the inter-particle volume). Therefore, they will elute at a higher retention time. On the contrary, larger molecules simply pass by some stationary phase pores as they are too large to enter them. Therefore, larger molecules elute through the column faster than smaller ones. [81]. In this work, the stationary phase was composed of Sepharose 4B packed inside a glass column, while the mobile phase was sterile PBS 1X, which flows through the column driven by gravity (manual operation). The column is shown in **Fig. 24**.

Figure 24. The SEC column used during the experiments.

The column was loaded with 2 mL of sample and then refilled with sterile PBS 1X to avoid drying. The collection of the eluate started 14 minutes after sample loading. A 96-well plate with transparent bottom was used to collect the eluate – every well was filled with four drops of the eluate. A minimum of 18 samples (6 wells × 3 rows) were collected. After the collection, the three samples that presented the "milkiest" aspect were selected and analysed independently.

2.2.4 – Dynamic Light Scattering (DLS)

DLS is a technique that can determine the size distribution profile of small particles in suspension. Indeed, the particles in suspension have a random fluctuation, also termed Brownian motion, which is stirred up by the collisions with the solvent molecules. The Brownian movement depends on particle size, temperature, and viscosity of the system. Thus small particles present quicker diffusion than bigger ones. Therefore, the dimensions of spherical particles are evaluated according to their hydrodynamic diameter, correlated with the Translational Diffusion Coefficient (*D*), which corresponds to the size of a sphere that diffuses at the same rate as the particle being measured. However, the limit of the DLS technique is to assume that all particles have a spherical shape. This means that the size of non-spherical particles cannot be accurately determined using this technique. If the shape of a particle changes to affect the diffusion speed, then the hydrodynamic size will change. In return, spherical particles can "appear" to have the same hydrodynamic diameter of aspherical particles of different volumes if their measured *D* are identic.

In the DLS technique, the size of the particles is inferred through the analysis of the light scattered by the particles moving in solution. Particularly, when the monochromatic light beam encounters the particles, the incident light scatters in all directions and a detector analyses the scattered light. Then, an autocorrelator function correlates the intensity of fluctuations of the scattered light concerning time, giving rise to an auto-correlation curve. The faster the curve reaches zero as a correlation value, the smaller the particles are. Indeed, the time when the curve starts to decay indicates the mean size of the particles. Moreover, the gradient of the curve is an indicator of the polydispersity of the sample. **Fig. 25** shows two typical correlograms from samples containing large and small particles.

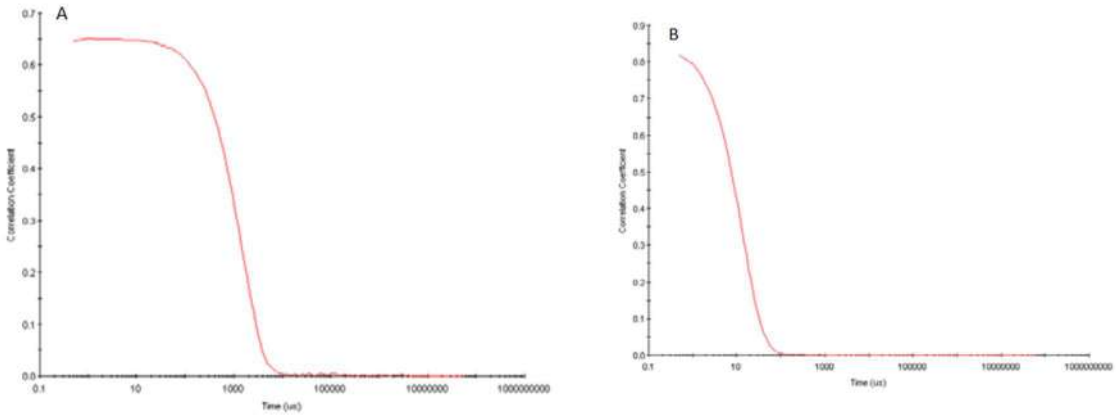

Figure 25. Typical correlogram from a sample containing bigger (A) and smaller (B) particles. The time at which the curves start to decay is different, and this can be related to the dimension of the particles. When the sample presents bigger particles (A), the correlation of the intensity of fluctuation starts to decay later owed to low particle fluctuation. Moreover, in these cases, the gradients of the curves imply monodisperse samples since they decay uniformly until they reach zero.

To determine the precise hydrodynamic diameter, *D* is extracted from the auto-correlation curve and then used in the Stock-Einstein equation (**Eq. 2)** to get the size of the particles:

$$d_h = \frac{kT}{3\pi\eta D} \qquad \textit{Eq. 2}$$

Where T and η refer to the known temperature and viscosity of the system, respectively, while k indicates the Boltzmann's constant [82].

Experimental details: All samples were analysed with a Zetasizer Ultra (Malvern Panalytical), and data were analysed using the ZS Explorer software, then elaborated by OriginPro® 2021. The instrument has a He-Ne laser at a wavelength of 633 nm, and the detector angle θ was set at 90 degrees for all the measurements to determine the forward scattering (**Fig. 26**). Before analysis, nanoparticle samples were diluted in PBS 1X for a final concentration of 0.2 mg/mL. 1 mL of diluted sample was then loaded into a polystyrene cuvette for the DLS analysis.

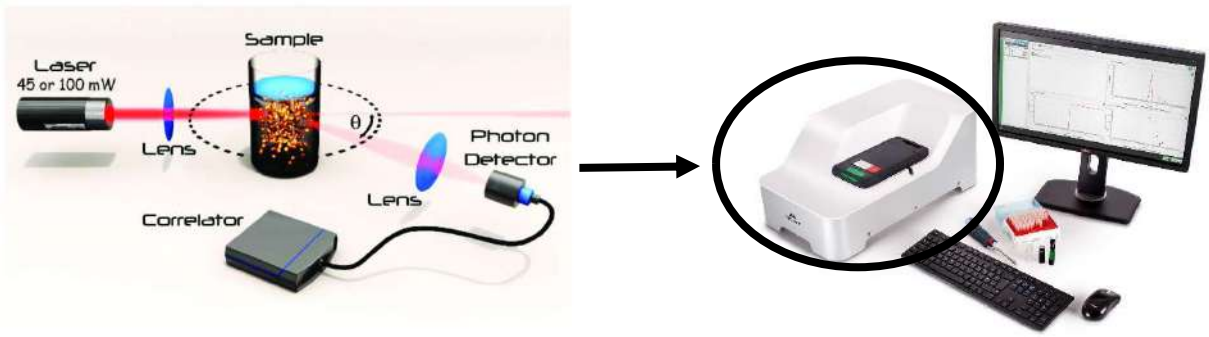

Figure 26. On the left, it is schematised the interior of the Zetasizer Ultra: the source of the laser, a first lens that focuses the beam, a second one that acts as a filter for the detector, and finally, the correlator [83].

2.2.5 – Transmission Electron Microscopy (TEM)

TEM is a high-resolution technique that uses a beam of electrons to produce detailed images of the analysed samples instead of light rays. This technology became possible after experiments on electron beams confirmed the De Broglie hypothesis of 1927 when it was first proposed that electrons behave as waves [84]. Indeed, the exceptional resolution of the TEM, compared to the common light microscope, comes from the fact that the wavelength of electrons is 100,000 times shorter than that of light. By using TEM one can achieve a magnification one thousand times higher than that of an optical microscope. The TEM part dedicated to producing the electron beam is termed the electron gun. In this part of the microscope, a tungsten filament is heated to produce the electron beam, passing through the condenser system that focuses the beam on the object. Then, the electrons that have passed the specimen are focused by the image – production system, composed of objective aperture, intermediate, and projector lenses. Finally, the electron beam is converted by the image–recording system, consisting of a fluorescent screen for viewing and focusing the image and a digital camera for permanent records. The entire lenses system is kept under vacuum to avoid the collision between electrons and air molecules, which can deflect the former. The TEM apparatus is depicted in **Fig. 27**.

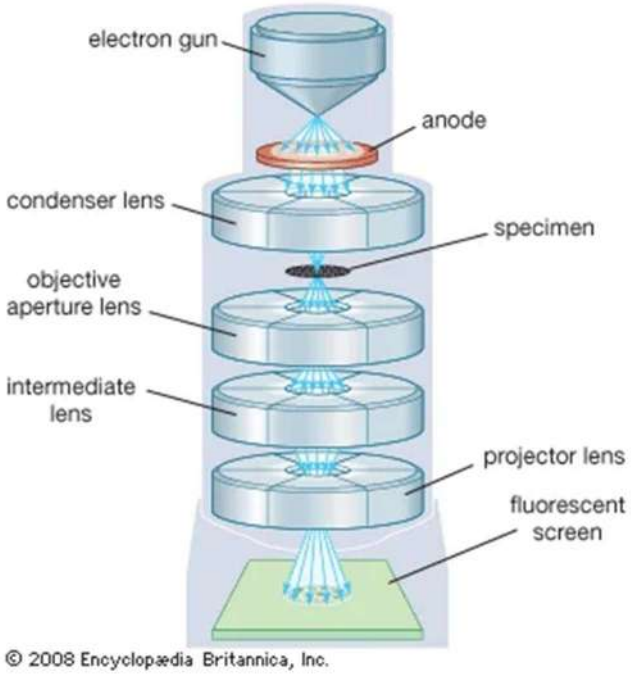

Figure 27. Transmission Electron Microscopy apparatus [85].

Experimental details: In this work, the morphology and size of the nanoparticles were analysed using a TEM JEOL J1010 at 80 kV equipped with CCD Megaview 1kx1k (**Fig. 28**). However, it is relevant to mention that just as any other technique, TEM also presents some limitations, including artefacts such as aggregation, particle collapse, and nonuniform deposition during the sample preparation [86].

The nanoparticle samples were diluted to a 1 mg/mL final copolymer concentration in water. Then, 5 μL of diluted sample was loaded on the TEM grid, which was previously glow-discharged for 30 seconds to render its surface hydrophilic. The sample was kept 1 minute on the grid before removing the excess with filter paper. Then, the grid was immersed into a PTA staining solution (0.5% p/v) for 3 seconds and immediately blotted again with filter paper. The grid was left dried at room temperature for at least 24 hours before using it.

Figure 28. TEM JEOL J1010 at IBEC.

3. RESULTS AND DISCUSSION

3.1 – Film hydration results

As stated above in section *1.3.2*, after the hydration of the copolymer film, the transition from lamellae to vesicles occurs. In this case, the transition was promoted by a vigorous and constant mechanical mixing which induced the swelling of the copolymer from the film. To study the evolution of this transition, the sample was analysed by DLS every week to reach a monodisperse vesicle population before purification by SEC. **Fig. 29** shows the correlogram curves of seven measurements made from the film hydration (week 0) before proceeding with the purification by SEC (week 6).

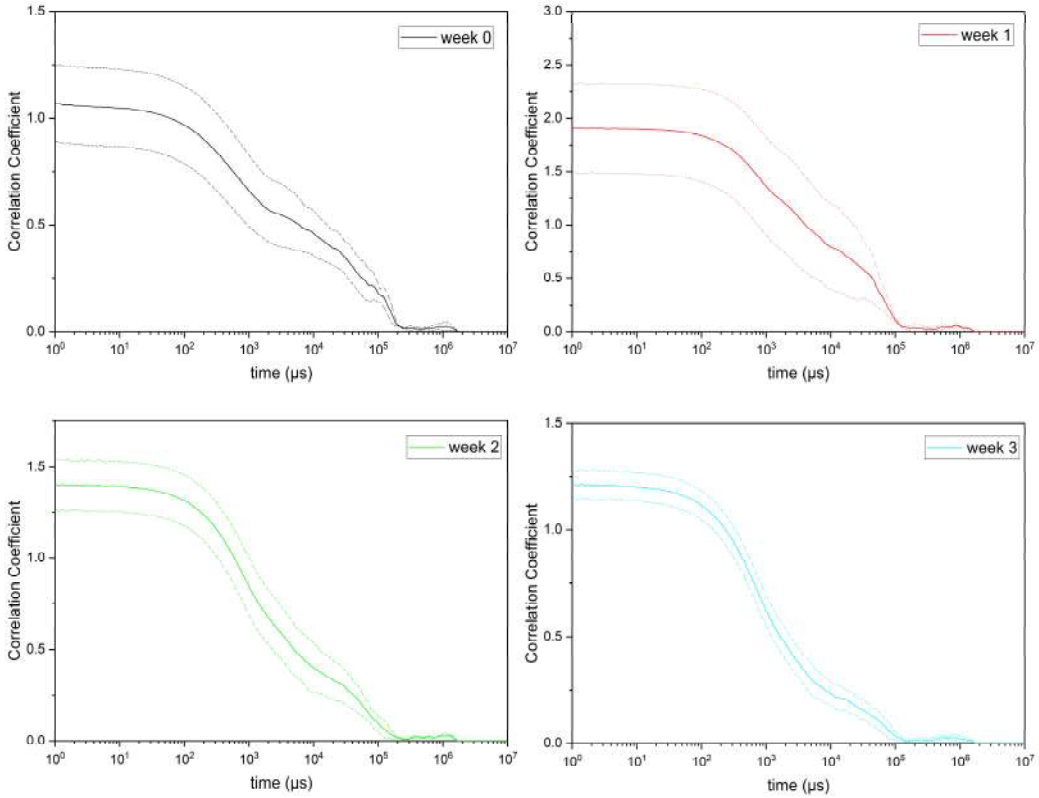

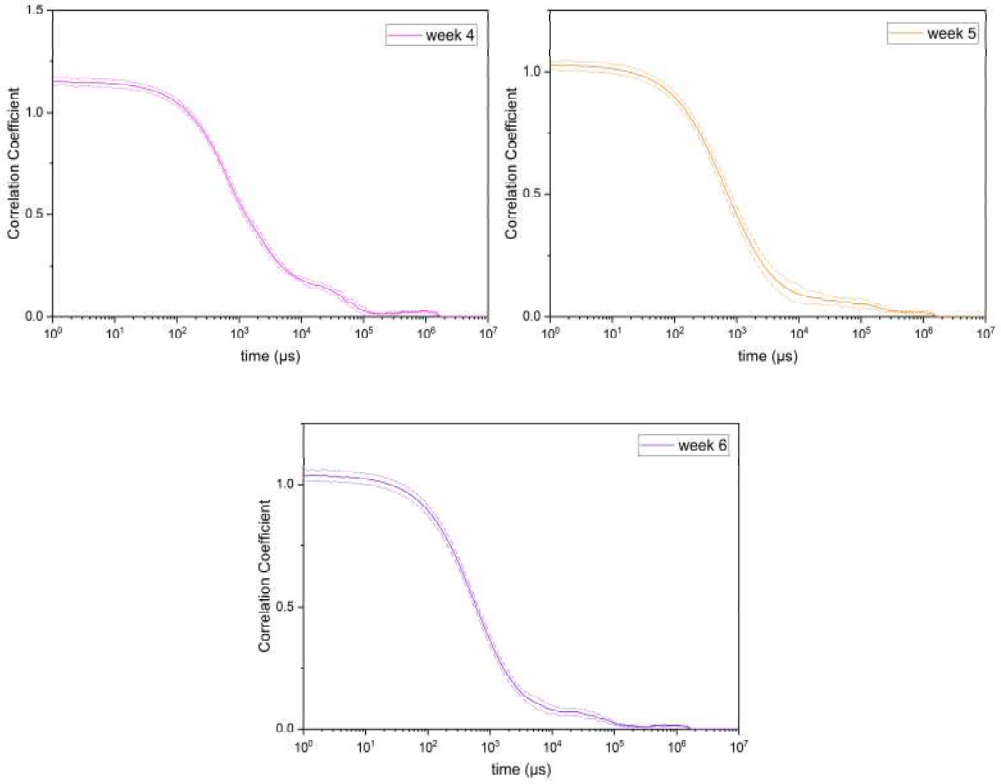

Figure 29. The seven correlation curves from week 0 (film hydration) to week 6 measured by DLS. Dotted lines represent the standard deviation of the measurements (N=3).

Such correlogram curves show an evident improvement in sample size and polydispersity throughout the six weeks. The week 6 curve starts with a correlation coefficient of about 1, an index of a perfect correlation in the first detected signals. Furthermore, the data of the three measurements show a low standard deviation, as seen by the dotted lines in the figures. Moreover, the correlation curve begins to decay earlier than the previous curves, indicating more small particles in the sample. The curve gradient also suggests a fairly low polydispersity, even though aggregates were detected as reported by the tail end of the curve. By week 6, the magnetic stirring was stopped, and the sample was purified by SEC to remove the aggregates. Therefore, the first collected fraction, mainly composed of bigger aggregates, was discarded, and the second and third fractions were collected and re-examined by DLS (**Fig. 30**).

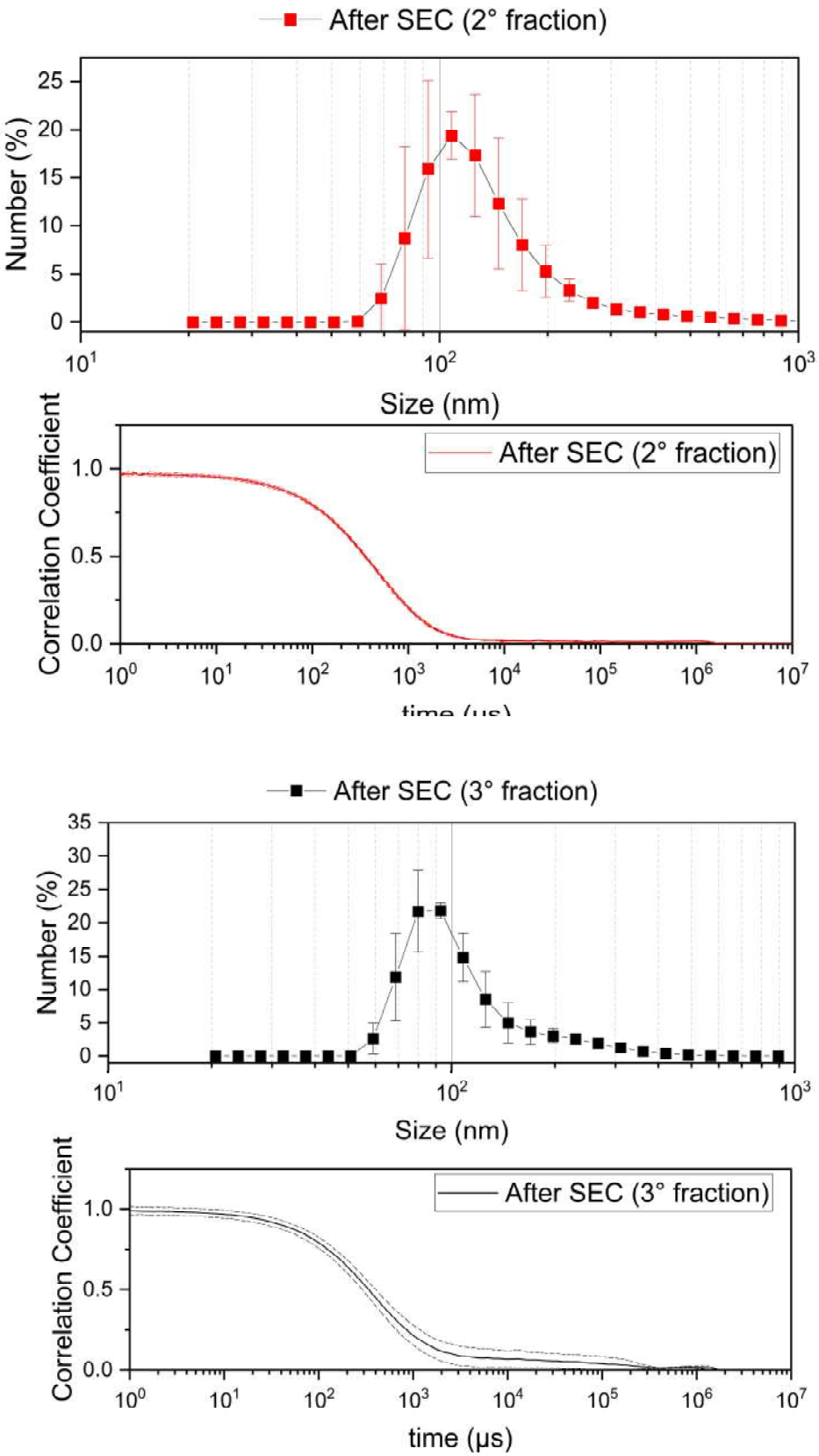

Figure 30. Distributions by number and correlation curves of second and third fractions collected after SEC. The sample was formulated via film hydration (N=3).

As expected, these distributions by number (**Fig. 30**) reveal a smaller NPs population in the third fraction than the second one. However, the third fraction still presents some bigger NPs, as shown by the tail end of the correlation curve and the distribution. It is important to mention that, in this case, the purification was carried out manually, with all the consequent technical limits, such as the incapability to precisely separate the diverse population of NPs. The size of the NPS and their morphology were further investigated in greater detail by TEM.

The first analysis of the sample by TEM was carried out after week 4 from the hydration of the copolymer film. **Fig. 31** shows a significant presence of tubular vesicles and already-formed closed vesicles. In this scenario, corroborated by the DLS (Fig. 29), the vesiculation process was ongoing since the tubular vesicles result from the mixing-related instability produced on the viscous lamellar phase. This means that the unbinding of membrane-bound compartments required further time to give rise to closed vesicles.

At week 6, the sample was observed again by TEM (**Fig. 32).** The high magnification image shows both well-formed closed vesicles and tubular vesicles, even though the latter were less in number, as confirmed by the DLS data (**Fig. 29**). As previously indicated, the film hydration was stopped at this point, with the confidence to have provided enough time for the vesiculation to occur and the ability to remove the bigger aggregates via SEC purification. Indeed, observing by TEM the sample after SEC purification, the image correspondent to the second SEC fraction contains both polymersomes with diameters ranging between 50 nm and 90 nm. A 140 nm long tubular vesicle on the point of topological change towards two closed vesicles (**Fig. 33**). Unfortunately, even though the third fraction showed a smaller NPs population by DLS analysis (**Fig. 30**), it was impossible to examine it by TEM due to technical problems.

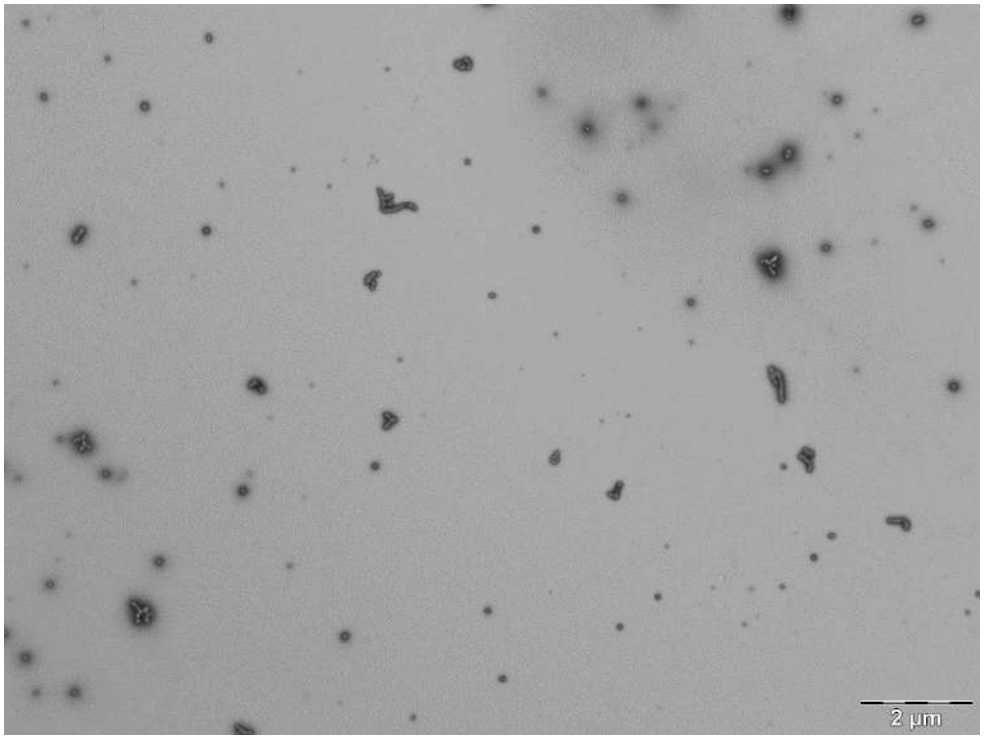

Figure 31. Low magnification image at TEM. Film hydration after 4 weeks.

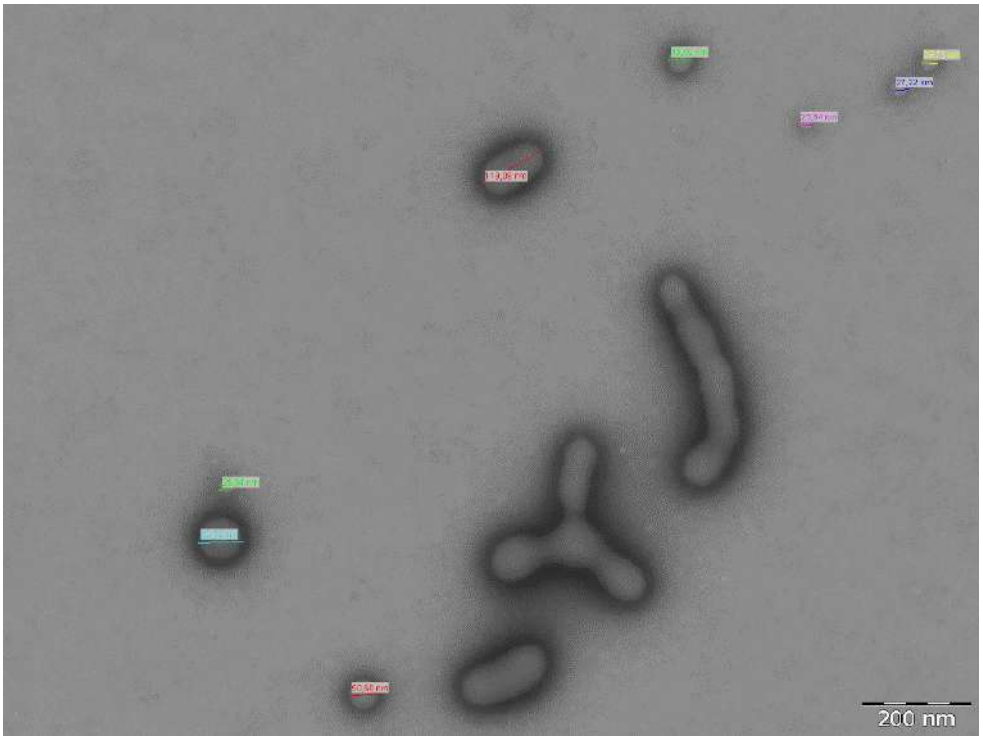

Figure 32. High magnification image by TEM. Film hydration after week 6, before SEC.

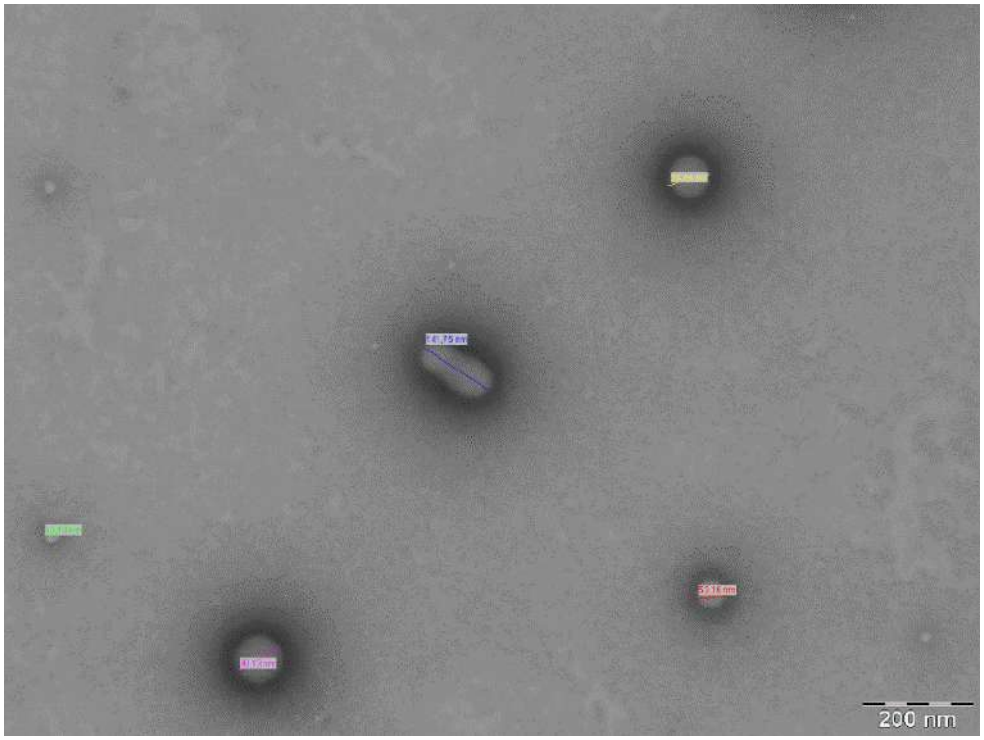

Figure 33. High magnification image by TEM. Film hydration after week 6, second fraction collected by SEC.

Although some improvements are needed to induce a homogeneous switch towards vesicular shapes, the film hydration showed to be a valid approach to formulate polymersomes with the desired diameter. Since the copolymer used was the $PMPC_{25}$-$PDPA_{80}$, the R* is about 20 nm (**Fig. 17**) [66], and consequently, the minimal desired diameter was 40 nm. $PMPC_{25}$-$PDPA_{80}$-based particles with a diameter below 40 nm are disk-like micelles, which are not ideal for the aim of this project. Therefore, we further investigated a bottom-up approach (solvent switch) in an attempt to increment particles size. Increasing polymersomes diameter and, consequently, the inner volume will theoretically permit the encapsulation of larger molecules, such as pDNAs, with higher encapsulation efficiency [87].

3.2 – Solvent-switch results

Since the film hydration method requires at least six weeks to give rise to a monodisperse vesicle population, a different approach was investigated to achieve the same result in a shorter time. The solvent-switch method allows complete solubilisation of the copolymer in an organic solvent, thus avoiding the kinetically-unfavoured copolymer swelling from the bulk, as in the film hydration. Changing from an organic solvent-based environment to an aqueous medium promotes faster vesiculation.

As reported in section *2.2.2*, several flow rates were investigated to study how the water-injection flow speed, which determines the solvent switch, influences the copolymer self-assembling. The first formulations were obtained with 20 mg/mL initial copolymer concentration. **Fig. 34** shows the DLS results of polymersome formulations at six different flow rates (0.5, 2, 5, 25, 50, and 100 uL/min). The experiments were performed after dialysis and before SEC purification.

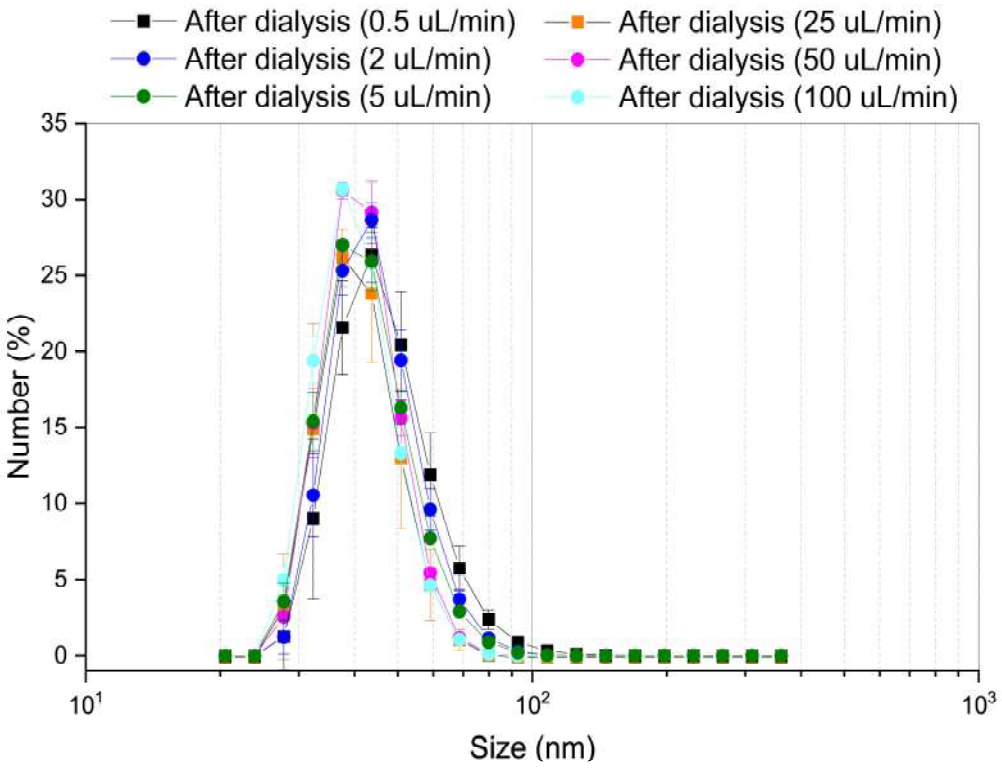

Figure 34. DLS analysis: overlapped size distributions by number of the six formulations at initial copolymer concentration of 20 mg/mL (N=3).

The overlap in the size distribution profile indicates an unexpected similarity amongst all formulations irrespective of the flow rate and despite the notable differences in terms of injection time. In this case, the volume of water injected was 1.15 mL, which means that at a flow rate of 0.5 uL/min, the injection lasted about 38 hours. On the other hand, when injecting at a flow rate of 100 uL/min, the process lasted about 12 minutes. Moreover, the mean diameter of all formulations was about 40 nm, which results incompatible with the minimum diameter that $PMPC_{25}$-$PDPA_{80}$-based polymersomes should have (**Fig. 17**) [66]. Indeed, as confirmed by TEM for the sample formulated at 2 μL/min (**Fig. 35**), most particles were disk-like micelles (diameter less than 40 nm) and not polymersomes.

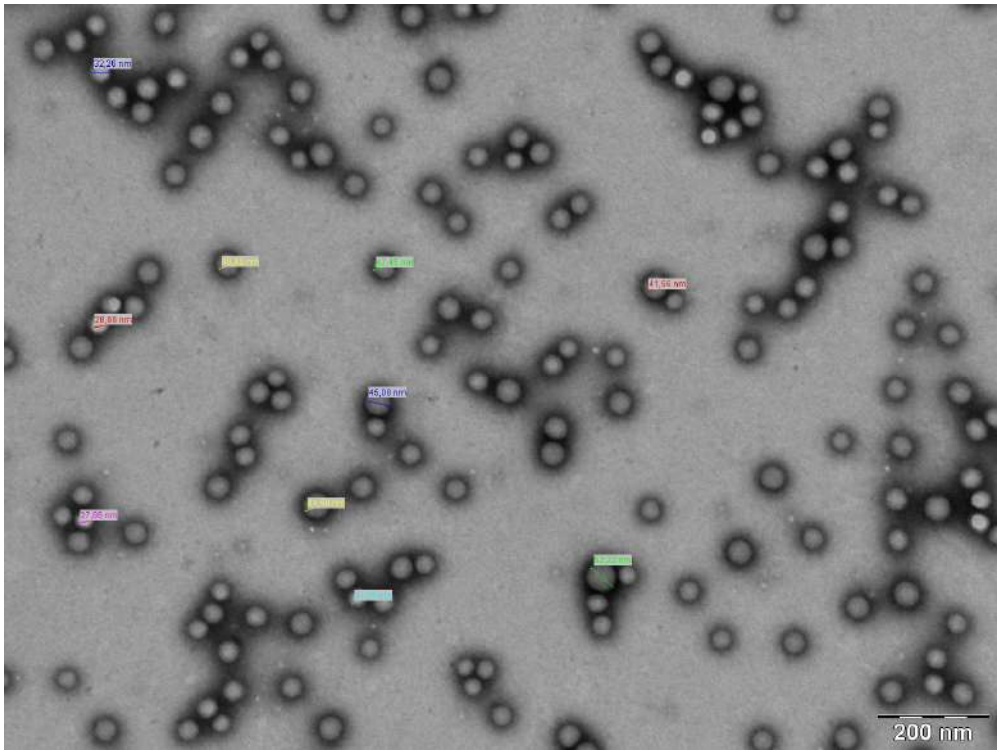

Figure 35. TEM image of the sample formulated with an initial copolymer concentration of 20 mg/mL and at a flow rate of 2 μL/min.

These results led to a change in another parameter that can influence the vesiculation process: the copolymer concentration. The following experiments were performed with an initial copolymer concentration of 2 mg/mL at six different flow rates. In **Fig. 36**, three comparisons of size

distributions are reported by a number between the samples formulated at the flow rates of 0.5 μL/min, 2 μL/min, and 5 μL/min, and copolymer concentrations of 2 mg/mL and 20 mg/mL.

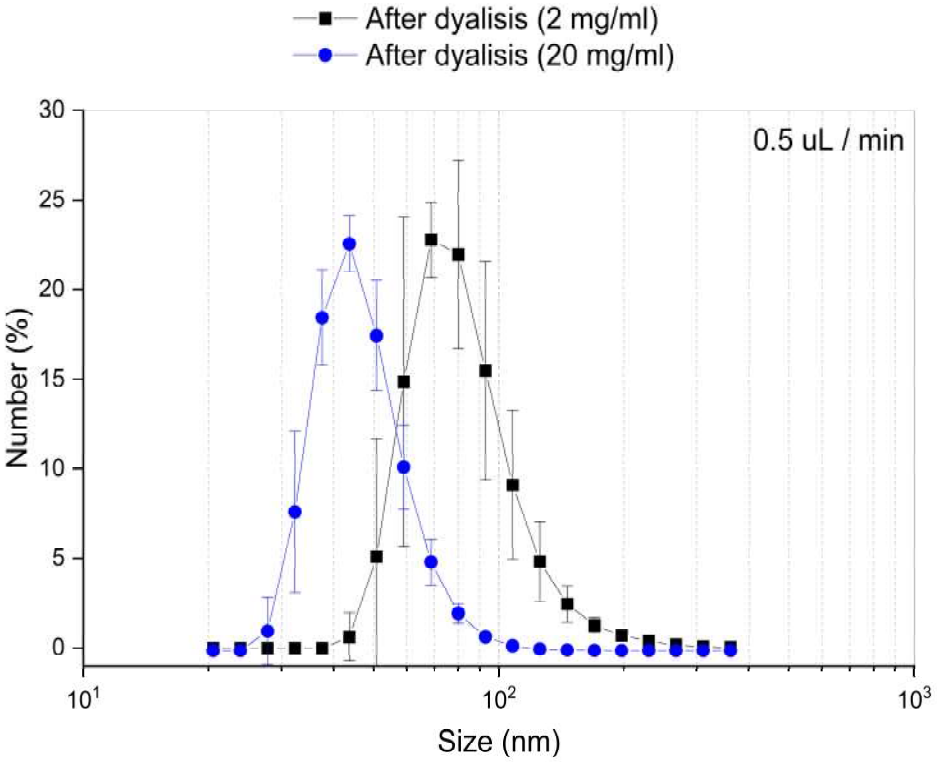

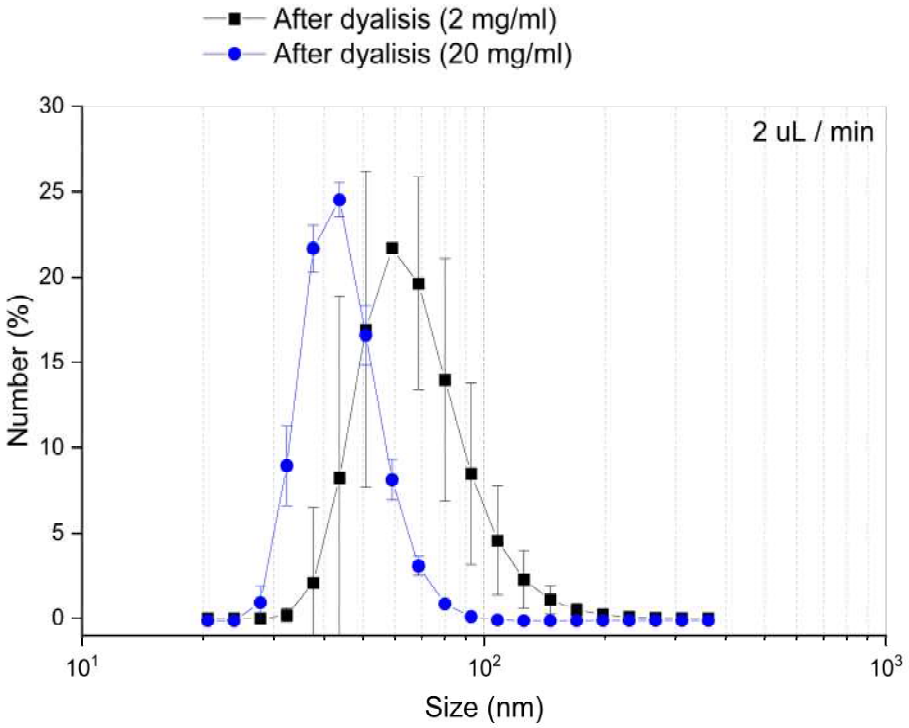

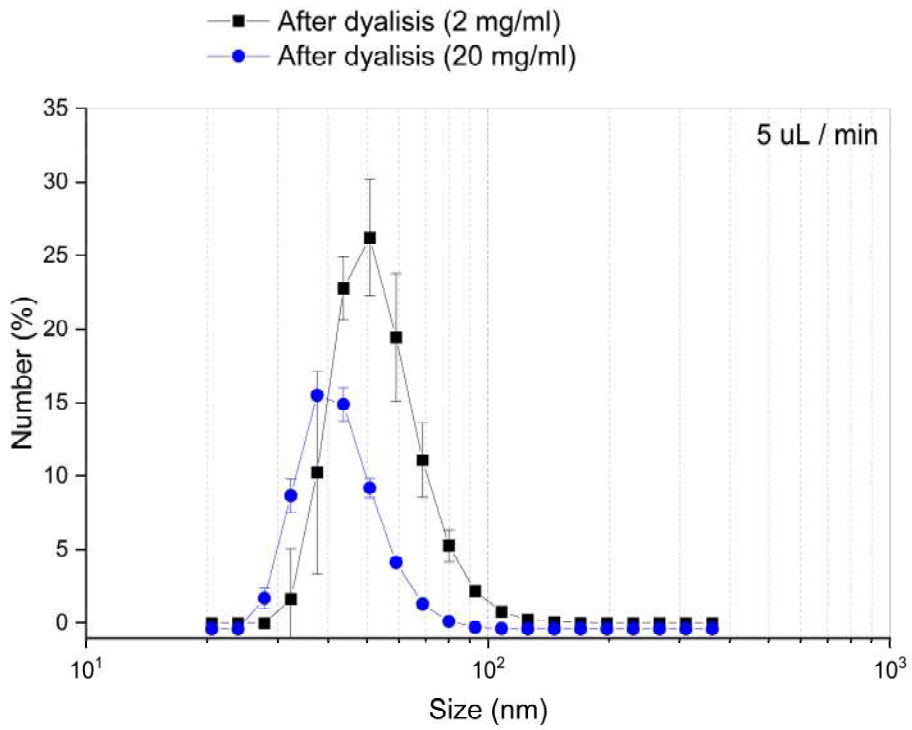

Figure 36. Size by number distribution between samples formulated at 0.5 μL/min, 2 μL/min, and 5 μL/min, and at different copolymer concentrations of 2 mg/mL and 20 mg/mL (N=3).

At the low concentration of 2 mg/mL, it is clear how the injection time/ flow rate influences the vesiculation process. At a flow rate of 0.5 μL/min, it is possible to obtain particles with a mean diameter of 80 nm, enough over the limit between disk micelles and polymersomes. This was also confirmed by TEM, as shown in **Fig. 37**.

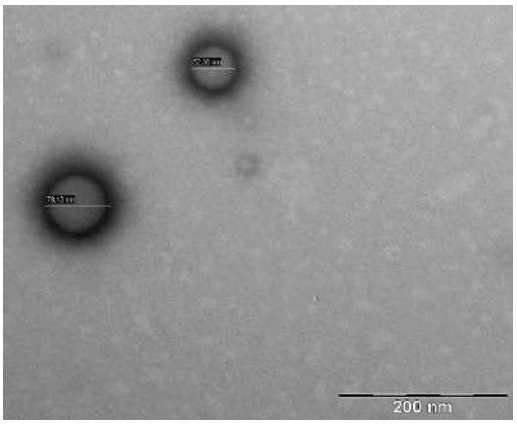

Figure 37. TEM image of polymersomes obtained via solvent switch at a copolymer concentration of 2 mg/mL and flow rate of 0.5 μL/min.

By increasing the flow rate, the mean diameter of the particles starts to decrease. Indeed, above the flow rate of 5 μL/min, it was noted that the mean diameter always remained around 40 nm, as observed for all the previous formulations at 20 mg/mL, indicating the presence of disk micelles instead of polymersomes. A comparison of all distributions by numbers of the formulations obtained at 2mg/mL is presented in **Fig. 38**.

Figure 38. Comparison of size distributions by number of the samples formulated at a copolymer concentration of 2 mg/mL and different flow rates (0.5, 2, 5, 25, 50, and 100 μL/min) (N=3).

Unfortunately, at a copolymer concentration of 2 mg/mL, the sample was transparent (compared to the milky aspect of samples at higher copolymer concentrations), which complicated the process of purification by SEC (it was too difficult to collect the eluate manually). Moreover, it is relevant

to point out that the concentration of every sample, after the injection of water into the copolymer solution, is decreased around 3 times (the volume of water was always 2.3 times the volume of the organic solvent). Therefore, the samples prepared at a 2 mg/mL copolymer concentration are too diluted for any following experiments. This can also be seen in **Fig. 37**, as it was challenging to find particles in the TEM grid.

Hence, the copolymer concentration was furtherly increased to 10 mg/mL. A flow rate of 0.5 μL/min was selected since it had demonstrated to give rise to polymersomes with the desired diameter. The formulation obtained was immediately analysed by DLS after the dialysis, before SEC purification. The size distribution by number and the correlation curve in **Fig. 39** reveal a mean diameter of 50 nm and the absence of aggregates.

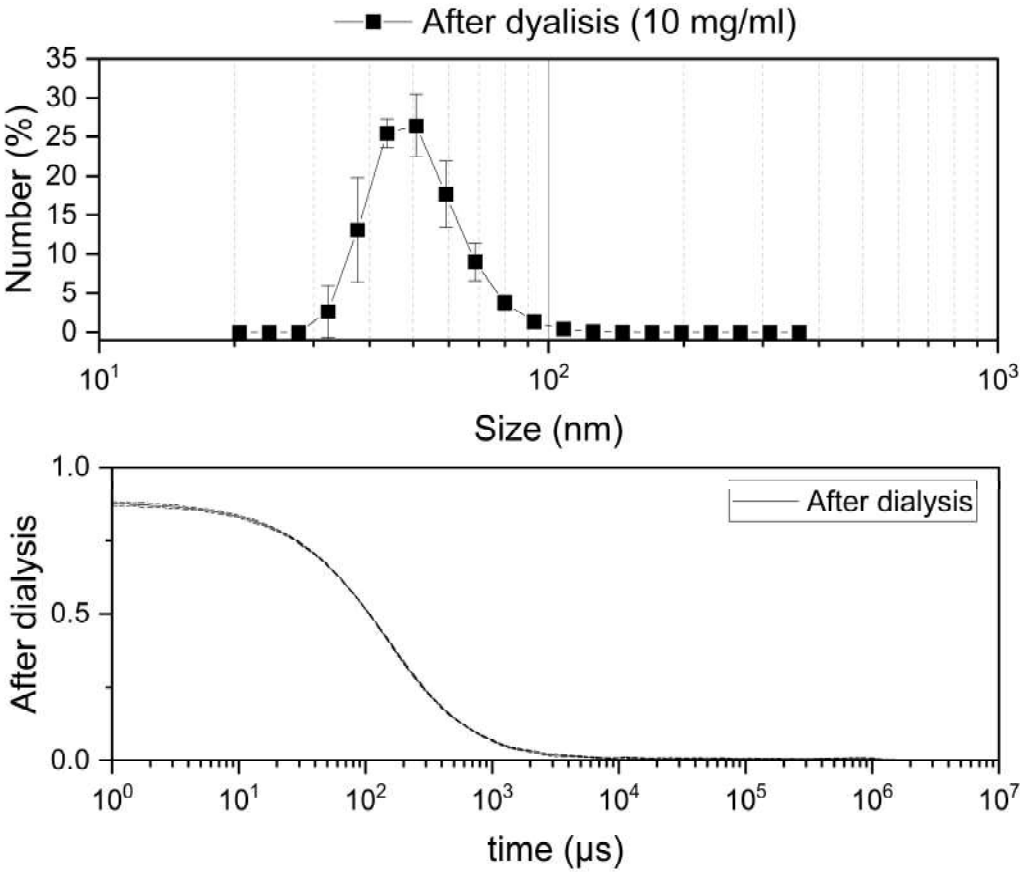

Figure 39. Size distribution by number and correlation curve of the sample prepared with an initial copolymer concentration of 10 mg/mL at a flow rate of 0.5 μL/min. DLS analysis was carried out after the dialysis (N=3).

Even though these results already suggested the presence of polymersomes in the sample, the sample was also analysed by TEM. Indeed, the images taken by TEM (**Fig. 40**) confirmed the DLS results: there was an abundant population of NPs (polymersomes) with a diameter greater than 40 nm.

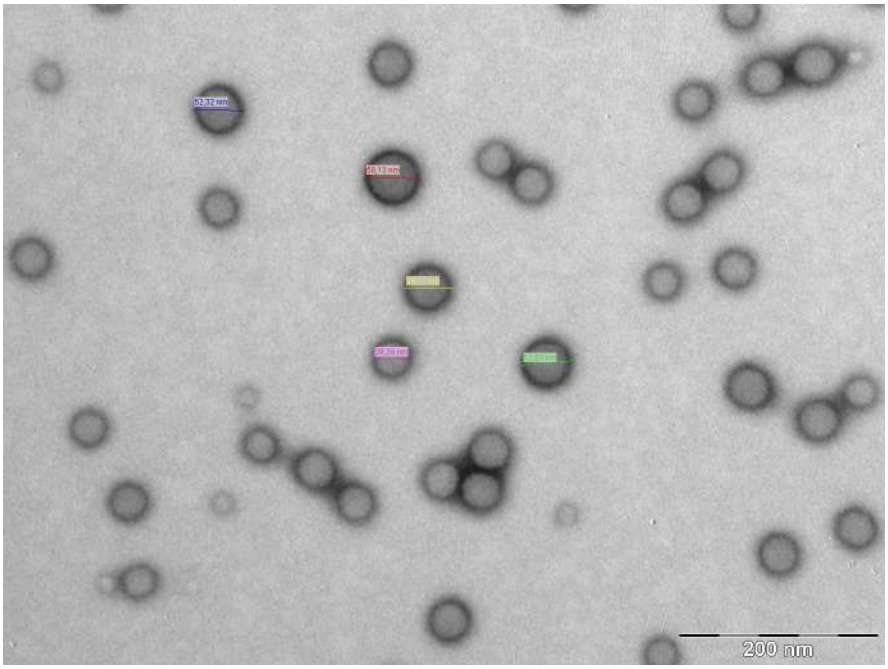

Figure 40. This image taken by TEM shows the presence of NPs with a diameter above 40 nm, *i.e.*, polymersomes.

To ultimately separate the polymersomes from the disk micelles, the sample was purified by the SEC by leveraging the difference of their dimensions. **Fig. 41** shows the size distributions by sample numbers formulated at a copolymer concentration of 10 mg/mL and a flow rate of 0.5 μL/min after dialysis, second fraction collected by SEC, and third fraction collected by SEC. It is evident how the polymersomes were differently distributed amongst the second and third fractions. The third fraction represents the ideal sample for this application with polymersomes with diameters ranging between 40 nm and 100 nm. Unfortunately, due to technical problems with the TEM instrument, it was impossible to analyse this sample by TEM.

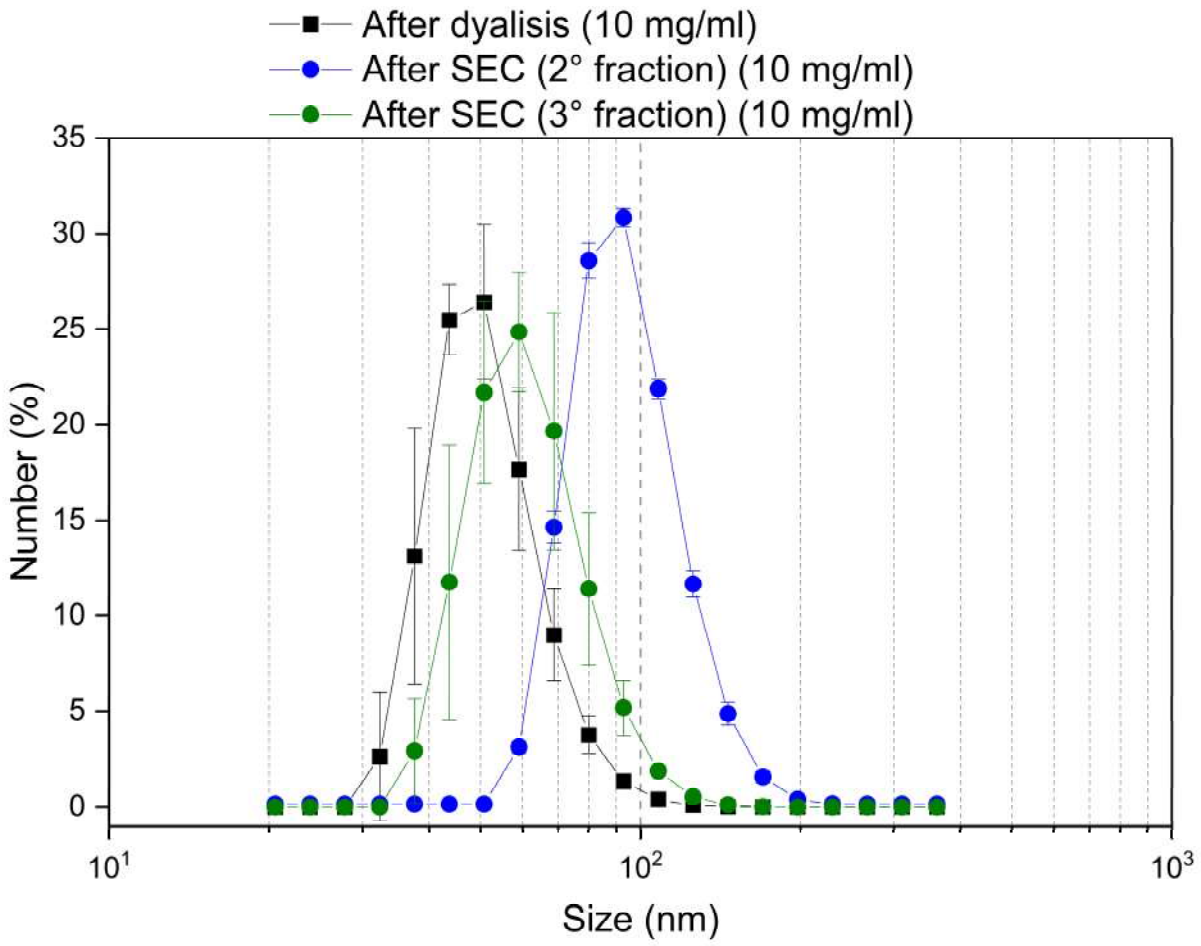

Figure 41. Comparison of size distributions by numbers between the sample after dialysis, second fraction collected by SEC, third fraction collected by SEC. The sample was formulated at a copolymer concentration of10 mg/mL and a flow rate of 0.5 μL/min (N=3).

The last step was to investigate the scalability of this process. Particularly, the idea was to double the volume of the final suspension after the injection. Therefore, the formulation with an initial copolymer concentration of 10 mg/ml and 0.5 uL/min was prepared using an initial organic volume of 1 mL and a water volume of 2.3 mL, as opposed to the volumes of 500 uL and 1.15 mL used in the previous experiments. After having dialysed the suspension, the latter was analysed by DLS and then compared with the respective previous formulation at a lower volume, as shown in **Fig. 42**. It is clear how the two distributions by number are very similar, demonstrating the possibility to scale up the process.

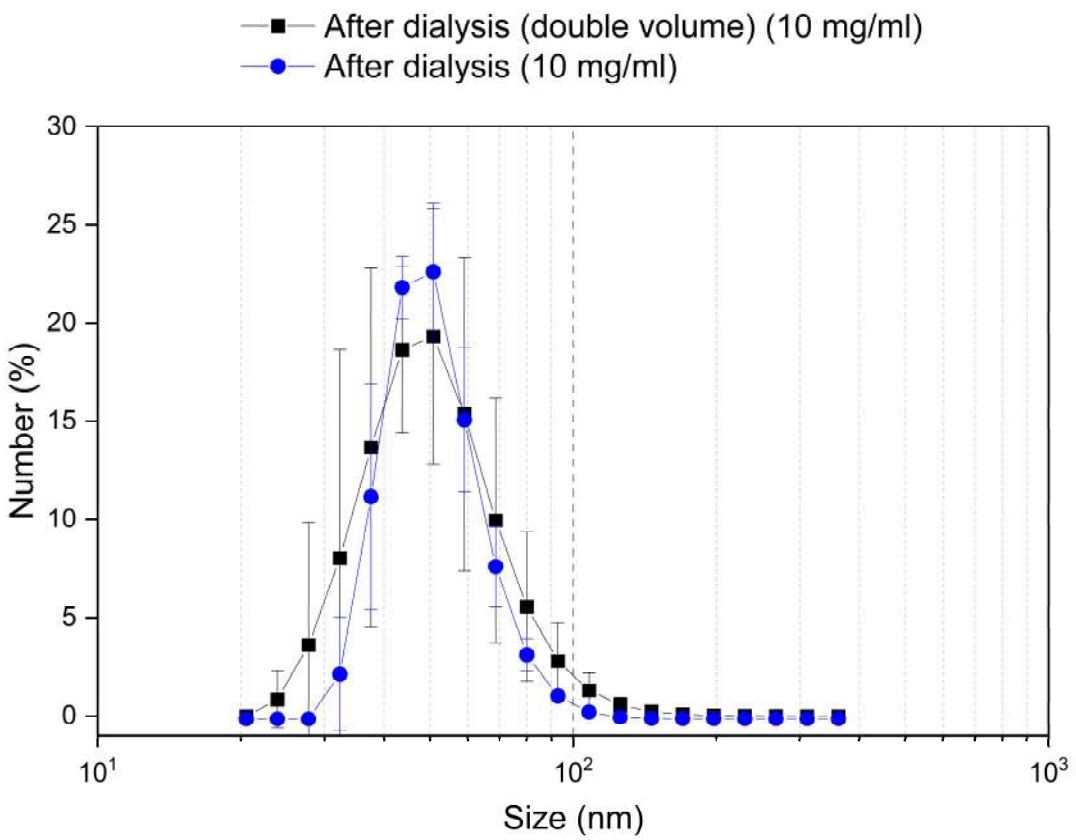

Figure 42. Comparison of size distributions by numbers between the previous formulation (volume of organic solvent of 500 uL and water of 1.15 mL) and the one obtained by doubling the volume of injected water and copolymer organic solution. The sample was formulated at a copolymer concentration of 10 mg/mL and flow rate of 0.5 μL/mL) (N=3).

4. CONCLUSIONS

This research aimed to develop an effective protocol to formulate polymersomes suitable for the delivery of pDNAs. Thanks to the macromolecular nature of their building blocks, polymersomes present improved mechanical proprieties and stability compared to their low-molecular-weight surfactant liposome counterparts. Polymersomes are expected to preserve the integrity of pDNAs by ensuring protection from biological agents, such as enzymes, which are ubiquitous in our organism [88]. To achieve that, polymersomes were formulated with the PMPC25-PDPA80, which provides a strong entanglement between the hydrophilic blocks, guaranteeing a stable vehicle for pDNAs [88].

In this thesis, two approaches for the formulation of polymersomes were investigated: film hydration and solvent switch. The solvent switch method was the most appropriate for this specific application, being faster and tuneable, allowing the formulation of polymersomes with the desired diameters above 40 nm. Slightly variations of diameter correspond to a considerable increment of inner volume, which could influence the encapsulation efficiency. However, the SEC purification protocol revealed reproducibility limits, being manually executed, something that can be overcome by using high-performance liquid chromatography in the following studies.

At higher copolymer concentrations of 20 mg/mL, the particles formed disk-like micelles with diameters around 40 nm. On the other hand, the formulations were too diluted at lower copolymer concentrations of 2 mg/mL. Increasing the flow rates above 5 μL/mL also resulted in the appearance of disk-like micelles, even at lower copolymer concentrations. Ultimately, the best formulation was at a 10 mg/mL copolymer concentration and flow rate of 0.5 μL/min, which provided polymersomes with dimensions between 40 and 100 nm. These PMPC-PDPA-based polymersomes will be further used in the following steps of the project to encapsulate pDNAs for transfection of glioma cells *in vitro*.

5. REFERENCES

1. Gazit, E. and A. Mitraki, *Plenty of room for biology at the bottom: an introduction to bionanotechnology*. 2013: World Scientific.
2. Wagner, V., et al., *The emerging nanomedicine landscape.* Nature Biotechnology, 2006. **24**(10): p. 1211-1217.
3. *Gene Therapy Clinical Trials Worldwide*. Available from: https://a873679.fmphost.com/fmi/webd/GTCT.
4. Tian, X., S. Angioletti-Uberti, and G. Battaglia, *On the design of precision nanomedicines.* 2020. **6**(4): p. eaat0919.
5. FDA, *What is Gene Therapy.* https://www.fda.gov/vaccines-blood-biologics/cellular-gene-therapy-products/what-gene-therapy#footnote1, 2019.
6. EMA, *Advanced therapy medicinal products: Overview.* https://www.ema.europa.eu/en/human-regulatory/overview/advanced-therapy-medicinal-products-overview.
7. Stephenson, M.L. and P.C. Zamecnik, *Inhibition of Rous sarcoma viral RNA translation by a specific oligodeoxyribonucleotide.* Proc Natl Acad Sci U S A, 1978. **75**(1): p. 285-8.
8. Sridharan, K. and N.J. Gogtay, *Therapeutic nucleic acids: current clinical status.* Br J Clin Pharmacol, 2016. **82**(3): p. 659-72.
9. Kulkarni, J.A., et al., *The current landscape of nucleic acid therapeutics.* Nat Nanotechnol, 2021. **16**(6): p. 630-643.
10. Zhou, J. and J. Rossi, *Aptamers as targeted therapeutics: current potential and challenges.* Nature Reviews Drug Discovery, 2017. **16**(3): p. 181-202.
11. Ruscito, A. and M.C. DeRosa, *Small-Molecule Binding Aptamers: Selection Strategies, Characterization, and Applications.* 2016. **4**.
12. Ni, S., et al., *Recent Progress in Aptamer Discoveries and Modifications for Therapeutic Applications.* ACS Appl Mater Interfaces, 2021. **13**(8): p. 9500-9519.
13. Zhu, G., *Aptamer–Drug Conjugates.* Bioconjugate Chemistry, 2015. **26(11)**: p. 2186-2197.
14. Liang, C., et al., *Tumor cell-targeted delivery of CRISPR/Cas9 by aptamer-functionalized lipopolymer for therapeutic genome editing of VEGFA in osteosarcoma.* Biomaterials, 2017. **147**: p. 68-85.
15. Ng, E.W., et al., *Pegaptanib, a targeted anti-VEGF aptamer for ocular vascular disease.* Nat Rev Drug Discov, 2006. **5**(2): p. 123-32.
16. Fire, A., et al., *Potent and specific genetic interference by double-stranded RNA in Caenorhabditis elegans.* Nature, 1998. **391**(6669): p. 806-11.
17. Bader, A.G., et al., *Developing therapeutic microRNAs for cancer.* Gene Ther, 2011. **18**(12): p. 1121-6.
18. Sendi, H., et al., *MiR-122 decreases HCV entry into hepatocytes through binding to the 3′ UTR of OCLN mRNA.* Liver Int, 2015. **35**(4): p. 1315-23.

19. Kristen, A.V., et al., *Patisiran, an RNAi therapeutic for the treatment of hereditary transthyretin-mediated amyloidosis.* Neurodegener Dis Manag, 2019. **9**(1): p. 5-23.
20. Syed, Y.Y., *Givosiran: A Review in Acute Hepatic Porphyria.* Drugs, 2021. **81**(7): p. 841-848.
21. Chakraborty, C., et al., *Therapeutic miRNA and siRNA: Moving from Bench to Clinic as Next Generation Medicine.* Mol Ther Nucleic Acids, 2017. **8**: p. 132-143.
22. Wolff, J.A., et al., *Direct gene transfer into mouse muscle in vivo.* Science, 1990. **247**(4949 Pt 1): p. 1465-8.
23. Sahin, U., K. Kariko, and O. Tureci, *mRNA-based therapeutics--developing a new class of drugs.* Nat Rev Drug Discov, 2014. **13**(10): p. 759-80.
24. Martini, P.G.V. and L.T. Guey, *A New Era for Rare Genetic Diseases: Messenger RNA Therapy.* Hum Gene Ther, 2019. **30**(10): p. 1180-1189.
25. Ran, F.A., et al., *Genome engineering using the CRISPR-Cas9 system.* Nat Protoc, 2013. **8**(11): p. 2281-2308.
26. Zangi, L., et al., *Modified mRNA directs the fate of heart progenitor cells and induces vascular regeneration after myocardial infarction.* Nat Biotechnol, 2013. **31**(10): p. 898-907.
27. Gao, Z., et al., *Mesenchymal stem cells: a potential targeted-delivery vehicle for anti-cancer drug, loaded nanoparticles.* Nanomedicine, 2013. **9**(2): p. 174-84.
28. Zimmermann, O., et al., *Successful use of mRNA-nucleofection for overexpression of interleukin-10 in murine monocytes/macrophages for anti-inflammatory therapy in a murine model of autoimmune myocarditis.* J Am Heart Assoc, 2012. **1**(6): p. e003293.
29. Kormann, M.S., et al., *Expression of therapeutic proteins after delivery of chemically modified mRNA in mice.* Nat Biotechnol, 2011. **29**(2): p. 154-7.
30. Pastor, F., et al., *An RNA toolbox for cancer immunotherapy.* Nat Rev Drug Discov, 2018. **17**(10): p. 751-767.
31. Bourquin, C., et al., *Immunostimulatory RNA oligonucleotides trigger an antigen-specific cytotoxic T-cell and IgG2a response.* Blood, 2007. **109**(7): p. 2953-60.
32. Corbett, K.S., et al., *SARS-CoV-2 mRNA Vaccine Development Enabled by Prototype Pathogen Preparedness.* bioRxiv, 2020.
33. Polack, F.P., et al., *Safety and Efficacy of the BNT162b2 mRNA Covid-19 Vaccine.* N Engl J Med, 2020. **383**(27): p. 2603-2615.
34. Ulmer, J.B., et al., *Induction of immunity by DNA vaccination: application to influenza and tuberculosis.* Behring Inst Mitt, 1997(98): p. 79-86.
35. Prompetchara, E., et al., *DNA vaccine candidate encoding SARS-CoV-2 spike proteins elicited potent humoral and Th1 cell-mediated immune responses in mice.* PLoS One, 2021. **16**(3): p. e0248007.
36. Liu, M.A., *A Comparison of Plasmid DNA and mRNA as Vaccine Technologies.* Vaccines (Basel), 2019. **7**(2).

37. MacGregor, R.R., et al., *First human trial of a DNA-based vaccine for treatment of human immunodeficiency virus type 1 infection: safety and host response.* J Infect Dis, 1998. **178**(1): p. 92-100.
38. Samal et al., *World's First Needle-Free DNA Vaccine's Emergency Approval in India.* Biotica Research Today, 2021. **3(8)**: p. 714-716.
39. Manghwar, H., et al., *CRISPR/Cas System: Recent Advances and Future Prospects for Genome Editing.* Trends Plant Sci, 2019. **24**(12): p. 1102-1125.
40. Mali, P., et al., *RNA-guided human genome engineering via Cas9.* Science, 2013. **339**(6121): p. 823-6.
41. Cong, L., et al., *Multiplex genome engineering using CRISPR/Cas systems.* Science, 2013. **339**(6121): p. 819-23.
42. Jiang, F. and J.A. Doudna, *CRISPR-Cas9 Structures and Mechanisms.* Annu Rev Biophys, 2017. **46**: p. 505-529.
43. Kyrou, K., et al., *A CRISPR-Cas9 gene drive targeting doublesex causes complete population suppression in caged Anopheles gambiae mosquitoes.* Nat Biotechnol, 2018. **36**(11): p. 1062-1066.
44. Zhou, H., et al., *Glia-to-Neuron Conversion by CRISPR-CasRx Alleviates Symptoms of Neurological Disease in Mice.* Cell, 2020. **181**(3): p. 590-603 e16.
45. He, Z.Y., et al., *In Vivo Ovarian Cancer Gene Therapy Using CRISPR-Cas9.* Hum Gene Ther, 2018. **29**(2): p. 223-233.
46. Durymanov, M. and J. Reineke, *Non-viral Delivery of Nucleic Acids: Insight Into Mechanisms of Overcoming Intracellular Barriers.* Front Pharmacol, 2018. **9**: p. 971.
47. Bulcha, J.T., et al., *Viral vector platforms within the gene therapy landscape.* Signal Transduct Target Ther, 2021. **6**(1): p. 53.
48. Xu, C.L., et al., *Viral Delivery Systems for CRISPR.* Viruses, 2019. **11**(1).
49. Chamundeeswari, M., Jeslin, J. & Verma, M.L., *Nanocarriers for drug delivery applications.* Environ Chem Lett 2019. **17**: p. 849–865.
50. Alvarez-Erviti, L., et al., *Delivery of siRNA to the mouse brain by systemic injection of targeted exosomes.* Nat Biotechnol, 2011. **29**(4): p. 341-5.
51. Mathiyalagan, P. and S. Sahoo, *Exosomes-Based Gene Therapy for MicroRNA Delivery.* Methods Mol Biol, 2017. **1521**: p. 139-152.
52. Gurunathan, S., et al., *Review of the Isolation, Characterization, Biological Function, and Multifarious Therapeutic Approaches of Exosomes.* 2019. **8**(4): p. 307.
53. Zhu, W., et al., *Exosomes derived from human bone marrow mesenchymal stem cells promote tumor growth in vivo.* Cancer Letters, 2012. **315**(1): p. 28-37.
54. Gilligan, K.E. and R.M. Dwyer, *Engineering Exosomes for Cancer Therapy.* Int J Mol Sci, 2017. **18**(6).
55. Willi Paul, C.P.S., *13 - Inorganic nanoparticles for targeted drug delivery.* In Woodhead Publishing Series in Biomaterials, 2020. **Biointegration of Medical Implant Materials (Second Edition)**: p. 333-373.

56. Chen, H.M. and R.-S. Liu, *Architecture of Metallic Nanostructures: Synthesis Strategy and Specific Applications.* The Journal of Physical Chemistry C, 2011. **115**(9): p. 3513-3527.
57. Wijaya, A., et al., *Selective Release of Multiple DNA Oligonucleotides from Gold Nanorods.* ACS Nano, 2009. **3**(1): p. 80-86.
58. Ma, P.a., et al., *Inorganic nanocarriers for platinum drug delivery.* Materials Today, 2015. **18**(10): p. 554-564.
59. Torchilin, V.P., *Lipid-Core Micelles for Targeted Drug Delivery.* Current Drug Delivery, 2005. **2**(4): p. 319-327.
60. Garavito, R.M. and S. Ferguson-Miller, *Detergents as tools in membrane biochemistry.* J Biol Chem, 2001. **276**(35): p. 32403-6.
61. Guimarães, D., A. Cavaco-Paulo, and E. Nogueira, *Design of liposomes as drug delivery system for therapeutic applications.* International Journal of Pharmaceutics, 2021. **601**: p. 120571.
62. Cabanillas, B., C.A. Akdis, and N. Novak, *Allergic reactions to the first COVID-19 vaccine: A potential role of polyethylene glycol?* 2021. **76**(6): p. 1617-1618.
63. Rideau, E., et al., *Liposomes and polymersomes: a comparative review towards cell mimicking.* Chemical Society Reviews, 2018. **47**(23): p. 8572-8610.
64. Hu, X., et al., *Stimuli-Responsive Polymersomes for Biomedical Applications.* Biomacromolecules, 2017. **18**(3): p. 649-673.
65. Guan, L., L. Rizzello, and G. Battaglia, *Polymersomes and their applications in cancer delivery and therapy.* 2015. **10**(17): p. 2757-2780.
66. Contini, C., et al., *Bottom-Up Evolution of Vesicles from Disks to High-Genus Polymersomes.* iScience, 2018. **7**: p. 132-144.
67. Massignani, M., H. Lomas, and G. Battaglia, *Polymersomes: A Synthetic Biological Approach to Encapsulation and Delivery*, in *Modern Techniques for Nano- and Microreactors/-reactions*. 2010. p. 115.
68. Battaglia, G. and A.J. Ryan, *Pathways of Polymeric Vesicle Formation.* The Journal of Physical Chemistry B, 2006. **110**(21): p. 10272-10279.
69. Battaglia, G. and A.J. Ryan, *The evolution of vesicles from bulk lamellar gels.* Nature Materials, 2005. **4**(11): p. 869-876.
70. Nagarajan, R., *Molecular Packing Parameter and Surfactant Self-Assembly: The Neglected Role of the Surfactant Tail.* Langmuir, 2002. **18**(1): p. 31-38.
71. Smart, T., *block copolymer nanostructure.* Nano Today, 2008.
72. Pearson, R.T., et al., *Effect of pH and Temperature on PMPC–PDPA Copolymer Self-Assembly.* Macromolecules, 2013. **46**(4): p. 1400-1407.
73. Shen, Y., et al., *Copolymer micelles function as pH-responsive nanocarriers to enhance the cytotoxicity of a HER2 aptamer in HER2-positive breast cancer cells.* Int J Nanomedicine, 2018. **13**: p. 537-553.

74. Jain, S. and F.S. Bates, *On the Origins of Morphological Complexity in Block Copolymer Surfactants.* 2003. **300**(5618): p. 460-464.
75. Kang, H., et al., *Size-Dependent EPR Effect of Polymeric Nanoparticles on Tumor Targeting.* Adv Healthc Mater, 2020. **9**(1): p. e1901223.
76. Ngoune, R., et al., *Accumulating nanoparticles by EPR: A route of no return.* Journal of Controlled Release, 2016. **238**: p. 58-70.
77. Cabral, H., et al., *Accumulation of sub-100 nm polymeric micelles in poorly permeable tumours depends on size.* Nature Nanotechnology, 2011. **6**(12): p. 815-823.
78. Prabhakar, U., et al., *Challenges and key considerations of the enhanced permeability and retention effect for nanomedicine drug delivery in oncology.* Cancer Res, 2013. **73**(8): p. 2412-7.
79. Nakamura, Y., et al., *Nanodrug Delivery: Is the Enhanced Permeability and Retention Effect Sufficient for Curing Cancer?* Bioconjug Chem, 2016. **27**(10): p. 2225-2238.
80. Albertazzi, L., et al., *Spatiotemporal control and superselectivity in supramolecular polymers using multivalency.* 2013. **110**(30): p. 12203-12208.
81. Fekete, S., et al., *Theory and practice of size exclusion chromatography for the analysis of protein aggregates.* Journal of Pharmaceutical and Biomedical Analysis, 2014. **101**: p. 161-173.
82. Stetefeld, J., S.A. McKenna, and T.R. Patel, *Dynamic light scattering: a practical guide and applications in biomedical sciences.* Biophysical reviews, 2016. **8**(4): p. 409-427.
83. Malvern. Available from: https://www.malvernpanalytical.com/en/products/technology/light-scattering/dynamic-light-scattering.
84. De Broglie, L., *Nouvelle dynamique des quanta.* Rapport et discussions du V^e Conseil de Physique Solvay, 1928.
85. Encyclopaedia Britannica, I.; Available from: https://www.britannica.com/technology/transmission-electron-microscope.
86. Parupudi, A., S.H.R. Mulagapati, and J.A. Subramony, *Chapter 1 - Nanoparticle technologies: Recent state of the art and emerging opportunities*, in *Nanoparticle Therapeutics*, P. Kesharwani and K.K. Singh, Editors. 2022, Academic Press. p. 3-46.
87. Wang, L., et al., *Encapsulation of Biomacromolecules within Polymersomes by Electroporation.* 2012. **51**(44): p. 11122-11125.
88. Lomas, H., et al., *Biomimetic pH Sensitive Polymersomes for Efficient DNA Encapsulation and Delivery.* 2007. **19**(23): p. 4238-4243.